swiss*nuclear*: PEGASOS Refinement Project:
SP2 – Ground Motion Characterization

Contract no. PMT-VT-1032

Seismic Shear Wave Velocity Determination and Hybrid Seismic Surveying at 20 Swiss Seismological Service Stations in Switzerland

Field Data Acquisition Period from 11th December 2008 until 18th June 2009

Summary Report

Client

swiss*nuclear*
Project PRP
Frohburgstrasse 17
4601 Olten

Contractor

GeoExpert ag
Seismic Prospecting
Oberfeldstrasse 6
8514 Amlikon-Bissegg

8603 Schwerzenbach, 24th July 2009

INDEX

PREAMBLE

List of terms and abbreviations

Naming

SN	**s**wiss**n**uclear as part of Swisselectric, the originating party
SED	**S**chweizerischer **E**rdbeben**d**ienst/Swiss Seismological Service
GE	**G**eo**E**xpert ag, contractor
SED station	Seismological monitoring station, operated by the SED
profile naming	09SN_17TORNY-S1 = 09: year SN: swissnuclear as customer 17: survey no. TORNY: SED station name S: s-wave survey; M: MASW; P: p-wave 1: profile 1

Methods

MASW surveying	**M**ultichannel **A**nalysis of **S**urface **W**aves; see sub-section 3.2 on page 17
refraction seismic surveying	Acquisition and processing of critically refracted seismic waves; see sub-section 3.3 on page 22
reflection seismic surveying	Acquisition and processing of reflected seismic waves; see sub-section 3.4 on page 27

Parameters

seismic p-wave velocity (v_p)
: Propagation velocity of compressional waves in rock material

$$v_p = \sqrt{\frac{K + \frac{4}{3}\mu}{\rho}}$$

with: K = Bulk modulus (= modulus of incompressibility)
μ = shear modulus (= modulus of rigidity)
ρ = density

seismic s-wave velocity (v_s)
: Propagation velocity of shear waves in rock material

$$v_s = \sqrt{\frac{\mu}{\rho}}$$

with: μ = shear modulus (= modulus of rigidity)
ρ = density

acoustic impedance (Z)
: Product of seismic p-wave propagation velocity (v_p) and rock/soil density (ρ);

$$Z = v_p \times \rho$$

the proportion of Z's of two layers is a measure of reflectivity

average velocity (v_{av})
: The mean velocity between surface and a particular depth is calculated by

$$v_{av} = z / t$$

with: z = depth
t = travel time of seismic wave to depth z

velocity scalar $v_{s,n}$
: The scalar value $v_{s,30}$ denotes the mean shear wave velocity between the surface to a depth of n = 30 meters;

$$v_{s,n} = \frac{\sum_{i=1}^{n} d_i}{\sum_{i=1}^{n} d_i / v_{si}}$$

with: d_i = thickness of layer i
v_{si} = corresponding shear-wave velocity.

Field Terms

source	Impulse device which generates controlled seismic energy in form of acoustic shock waves. Sources may be of the impact type as explosive charges, hammer blows, weight droppers and air guns. More sophisticated source types are vibrators which generate frequency and amplitude encoded source signals of a certain duration. In this project, hammer blows are used for generating both shear and compressional waves.
geophone	Device which converts ground movement (displacement) into voltage signals, which may be recorded at a receiver station. The deviation of the measured voltage values from the base line is called the seismic response and is analyzed for structure of the earth. In this project, analog horizontal (for shear wave detection) and vertical (for compressional shear wave detection) geophones are used.
A/D converter	Analog to digital converter, device for converting analog (voltage) signals recorded by the geophones into digital values for data storage and processing purposes.
array	Linear (1D) or areal (2D) lay-out arrangement of receiver stations
offset	Distance between the seismic source point and a particular receiver station
profile station	Position of a particular geophone station on the seismic profile
profile meter	Count of meters along the seismic profile; generally profile station ≡ profile meter (with 1 m station spacing)
x-t domain	2-dimensional plane in which seismic data are presented; the horizontal x-axis represents the profile distance along the surface, the vertical t-axis denotes the travel time of seismic signals.

Processing Terms

first break (FB) time	Manually or automatically determined traveltime of first seismic event from source to receiver; for near offset receivers, that is a direct wave traveling through the uppermost soil; for far offset receivers, that is normally a refracted wave; first break times are detectable for different wave types such as body waves (compressional and transverse waves) and with lower accuracy for surface waves.
TWT	**T**wo **W**ay **T**ime; time it takes for a seismic (source) signal generated at the surface to travel to the depth of a reflector or refractor and back to the surface
CDP / CMP	**C**ommon **D**epth **P**oint / **C**ommon **M**id **P**oint for horizontally layered formations CDP ≡ CMP
NMO	**N**ormal **M**ove **O**ut correction, travel time correction for the horizontal alignment of reflection events situated on a reflection hyperbola in the x-t domain.
RMS	Root Mean Square, a statistical measure of the magnitude of varying quantity.

Interpretation Specifics

seismic velocity field	Distribution of the intrinsic seismic wave velocities in the subsurface
seismic section	Display of the seismic data along a seismic profile consisting of numerous seismic traces with location given along the x-axis and TWT or depth along y-axis.
reflection event	Signal arrival visualizing an impedance contrast; normally interpreted as a lithological or geomechanical boundary.

1 INTRODUCTION

1.1 Survey objectives

The seismic survey's main task is to determine the distribution function of the shear wave velocities in the depth interval of the uppermost 30 m along 100 m long seismic profiles.

Additionally, the following objectives are to be met:

- the mapping of the topography of the rock face, i.e. the thickness of the Quaternary deposits;
- the determination of the thickness of the weathered zone and its degree of decompaction at the bedrock surface;
- a general view of geological structures.

1.2 Methodology

Seismic waves are acoustic signals traveling in elastic rock material. They can be divided in the two groups of a) body waves (compressional and transverse or shear waves) and b) surfaces waves (Rayleigh and Love waves). The body waves are traditionally used to map the rock density and elastic properties as well as structural inhomogeneities in the subsurface. Surface waves, until recently rated as unavoidable self generated noise and having been treated as such, have seen a revival, because their information content can now be extracted thanks to the advances in modern data acquisition and processing tools. The analysis of the amplitude spectra of surface waves of the Rayleigh type provides a fairly accurate measure of the shear wave velocity distribution in the depth range between 5 m and 100 m.

This summary of the selected surveying methods gives an overview over the applied seismic methods for meeting the survey objectives. Please refer to the detailed processing description further below (chapter 3).

1.2.1 Multichannel analysis of surface waves (MASW)

In multichannel analysis of surfaces waves, the two basic facts that a) surfaces waves are dispersive and b) the surface wave velocity depends on shear wave velocity are used to derive a shear wave velocity section.

Dispersion is the phenomenon in which the phase velocity of a seismic event depends on the frequencies contained in the signal. A rainbow is a familiar example of dispersion. A plot of phase velocities vs. frequency (so called dispersion image resp. dispersion curves when frequencies are allocated to specific phase velocities) allows to get conclusions about the subsurface shear wave velocity field. In a geological setting, the velocities normally increase with increasing depth, so the velocity effect of lower frequencies allows velocity calculation on greater depth.

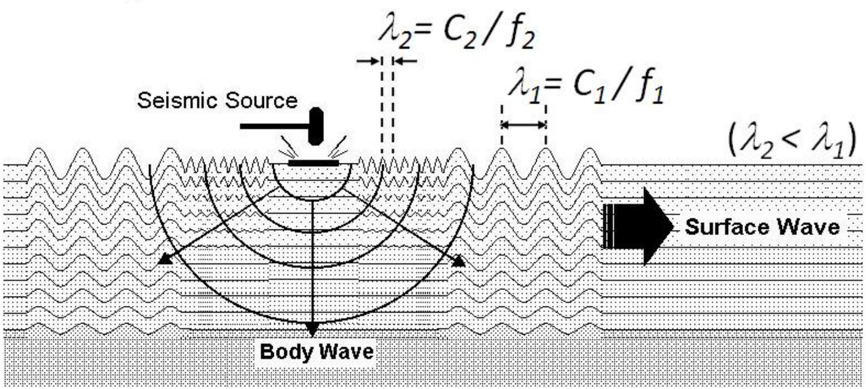

Fig. 1.2a: Schematic image of source-generated surface waves with wavelength λ in relation to the phase velocity c and the frequency f. (image from www.masw.com)

The basis for the inversion process is the assumption that s-wave velocities fundamentally control changes in Rayleigh-wave phase velocities for a layered earth model. Poisson's ratio, density and p-wave velocity have a reduced ascendancy on the phase velocities. The complete inversion algorithm can be found in Xia et al. (1999).

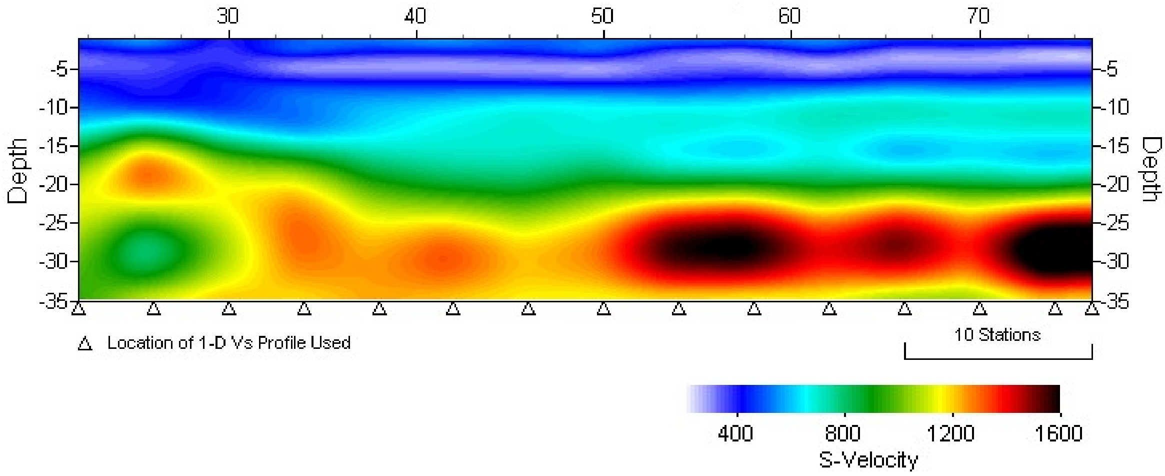

Fig. 1.2b: MASW-processed shear wave velocity fields as the result of surface wave analysis.

1.2.2 Refraction seismic surveying

In analogy with the laws in optics that govern the refraction of rays of light at the boundaries between two layers with differing propagation velocities of light (Snell's Law, Fig. 1.2c), seismic rays with an angle of incidence greater than the critical angle from the vertical cannot penetrate the layer below, resulting in the total refraction of the ray at the layer boundary. The totally refracted seismic wave then travels along the surface of the hard layer and continuously emits part of its signal back to the earth's surface.

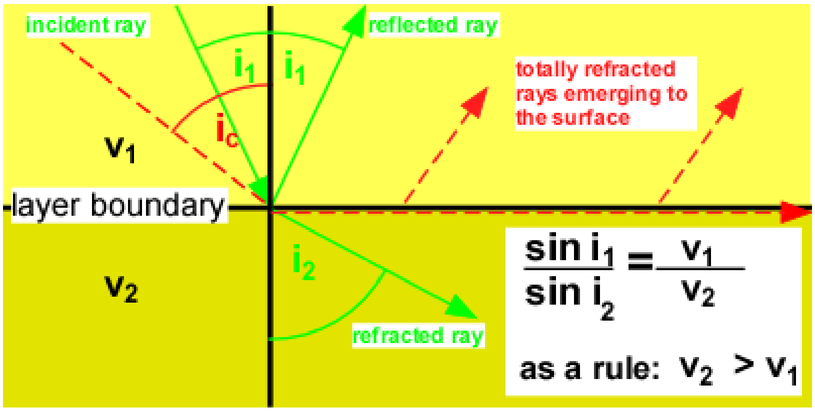

Fig. 1.2c: Reflection and refraction of seismic raypath at the interface between a soft layer above a hard layer below. The raypath with the angle of incidence i_1 at the interface is deflected from the vertical at a larger angle i_2 from the vertical when it enters the hard layer below with the higher velocity v_2. As the angle of incidence i_1 approaches the critical angle i_c the angle of emergence i_2 becomes 90° with the result that the seismic wave is totally refracted and cannot penetrate the layer below.

Fig. 1.2d portrays the trajectory of the wave paths of the seismic source signal in the sub-surface. Depending on the ray's angle of incidence with the interface, part of the acoustic energy travels as a totally refracted wave along the interface boundary and continuously emits energy back to the surface.

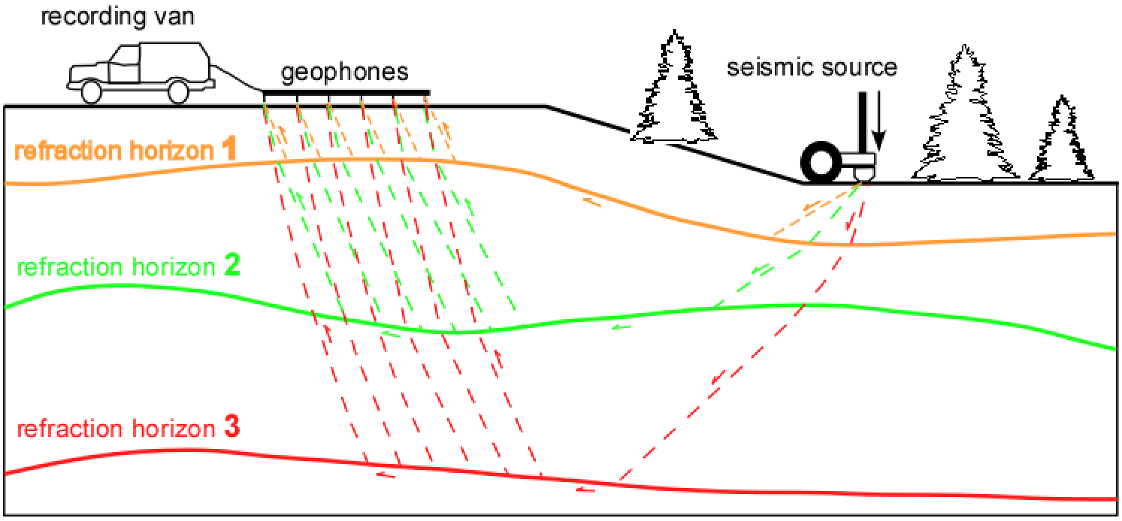

Fig. 1.2d: The field set-up and the ray paths trajectories of a refraction survey.

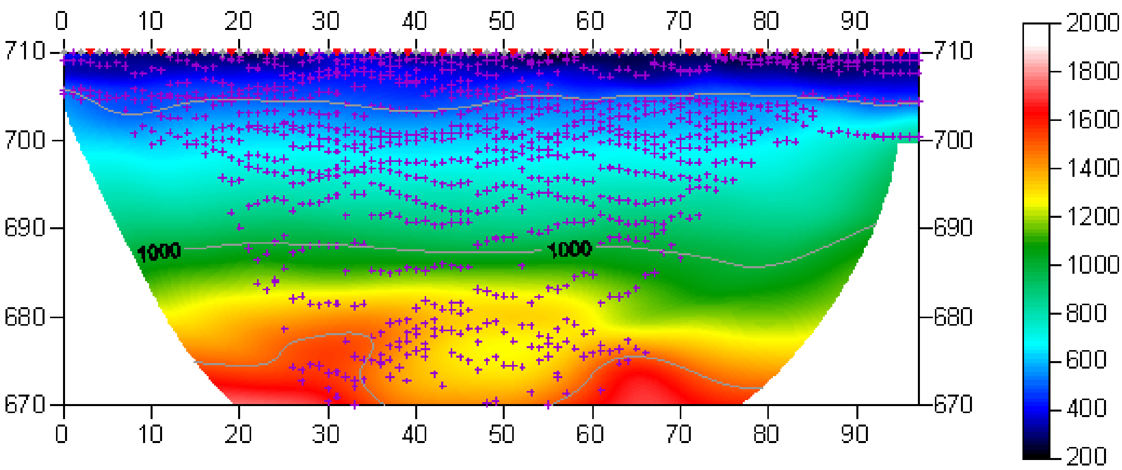

Fig. 1.2e: The seismic velocity section as a result of a refraction seismic survey.

1.2.3 Reflection seismic surveying

The underlying principle in reflection seismic profiling is identical with the one with the echo sounder on a ship: A source signal generated at the surface penetrates the ground in a vertical or near vertical direction. At layer boundaries, i.e. at interfaces of velocity contrasts, the signal is reflected back to the surface – like in the case with the signal of the echo sounding device at the sea bottom. Unlike the echo sounding technique, where the transmitter and the receiver are assembled into one unit at the ship's bottom, in seismic reflection surveys there is an arrangement of a large number of receivers (geophones) which record the signal emitted from a single source position (see Fig. 1.2f).

The recording arrangement consists of a number of geophone stations laid out at regular, equidistant spacings with the source point usually in the middle – or moving along the geophone layout – of the spread. As with refraction seismic tomography, the seismic source may be of an impact type (hammer, weight dropper) or explosives fired in shallow boreholes.

In this manner, reflection points on layer boundaries at various depths in the subsurface are sampled by a multitude of transmitter-receiver configurations resulting in a so-called multiple coverage of seismograms at each reflection point position.

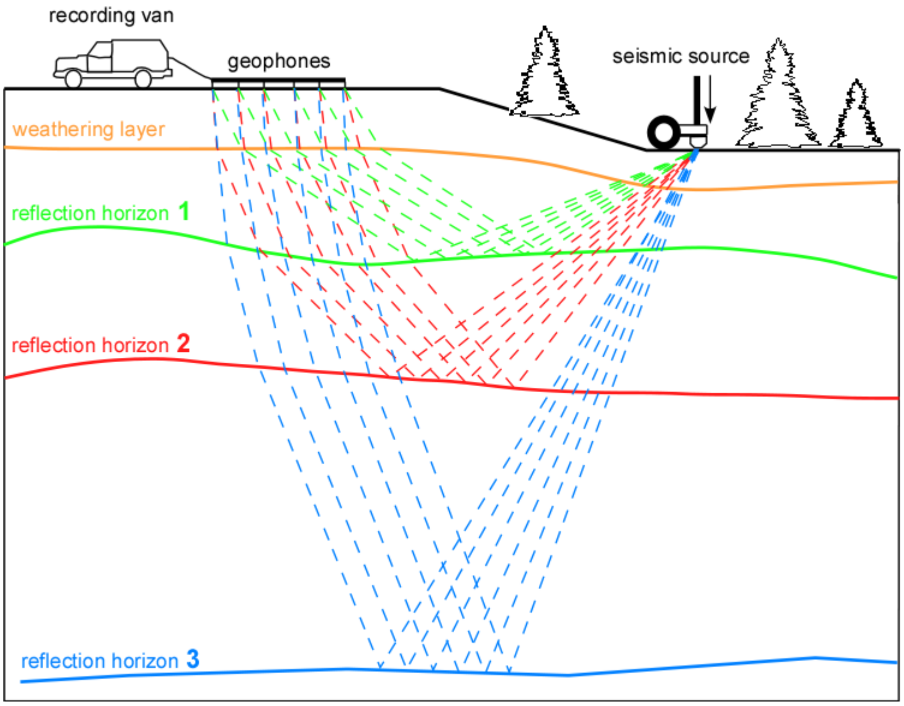

Fig. 1.2f: Schematic presentation of the seismic reflection geometry of ray paths.

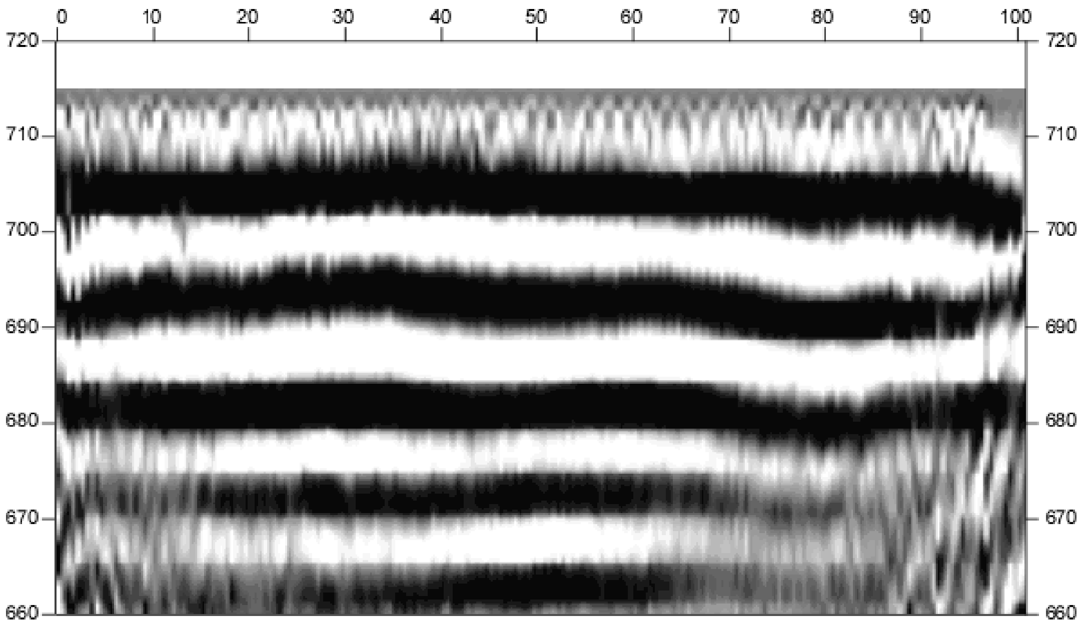

Fig 1.2g The seismic depth section as the result of reflection surveying images the reflectivity of sub-surface structures.

1.2.4 Hybrid seismic sections

Reflection seismic profiling as well as refraction diving wave tomography, when applied as the sole prospection methods, have their undisputed merits in their performance, but unfortunately also some shortcomings, depending on the objectives of each individual survey, as outlined in the table below.

Comparative performance summary of refraction tomography surveying and high resolution reflection seismic profiling

	Reflection seismic profiling	*Refraction diving wave tomography*
High resolution at shallow depths (< 10 m)	LIMITED	GOOD
High resolution at greater depths (> 20 m)	GOOD	LIMITED
Depth of investigation	HIGH	LIMITED
Rock / soil quality indicator & rippability	POOR	GOOD
Detection of velocity inversions	POOR	GOOD
Fault zone indicator	GOOD	LIMITED

Tab. 1.2: Comparison of advantages and drawbacks of seismic p-wave methods.

As an obvious conclusion from the above comparison of the capabilities of the two methods, it is desirable to combine their data acquisition and interpretation procedures.

Although the results of the reflection seismic data processing and the refraction tomography evaluation are based on the same data set, they are completely independent from each other, which enhances the reliability of a joint interpretation. The latter is further assisted by a suitable presentation of two results whereby the drawbacks of one method are compensated by benefits of the other.

An effective direct and comparative correlation is obtained by transparently superimposing the seismic velocity gradient field derived from refraction tomography onto the reflection seismic depth section (see Fig. 1.2f).

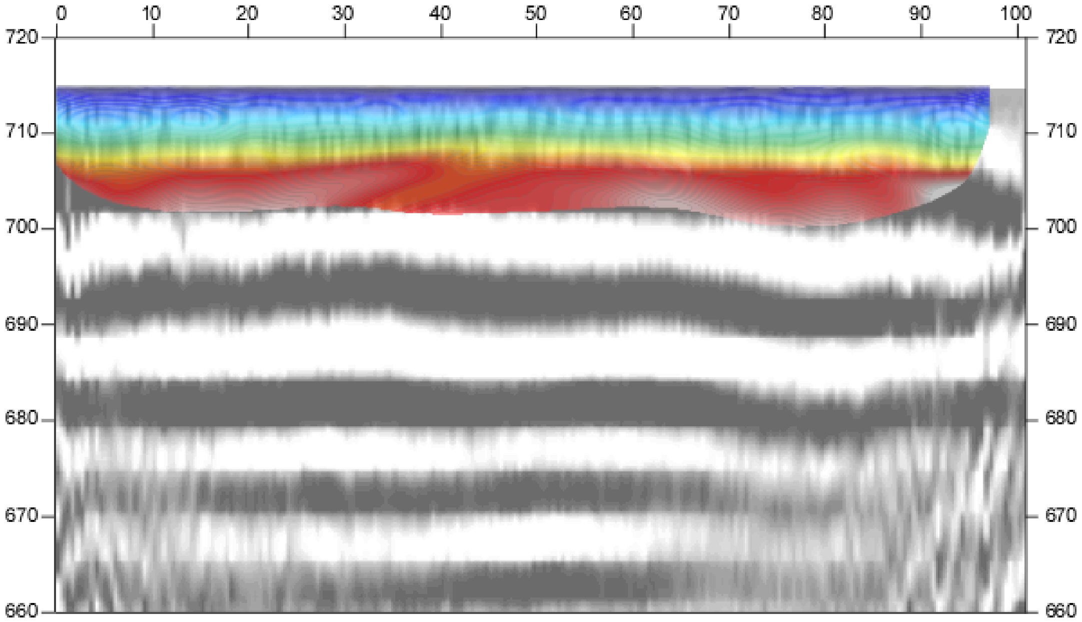

Fig. 1.2h The hybrid seismic section as the result of combined refraction and reflection seismic surveys.

1.3 The choice of the appropriate surveying methods

Several methods are available for deriving the s-wave velocity distribution in the subsurface at any given position:

- in-situ measurement by down-hole or crosshole seismic surveying;
- shear-wave refraction tomography profiling;
- dispersion analysis of surface waves (MASW; **M**ultichannel **A**nalysis of **S**urface **W**aves)

The surveys are to be carried out at, or as close as possible near some 20 SED earth quake monitoring stations in Switzerland. Ideally, the surveys are to be conducted on two orthogonal profiles in order to derive at their point of intersection a robust 1D s-wave velocity distribution function by correlation. To this end, the methods of MASW and shear-wave refraction tomography profiling are to be combined.

The results are to include the following fundamental parameters $v_{s,5}$, $v_{s,10}$, $v_{s,20}$, $v_{s,30}$, $v_{s,40}$, $v_{s,50}$, $v_{s,100}$ are to be calculated, also an error estimation of all values.

The data acquired for the MASW method are to be subjected to complementary **p-wave hybrid seismic data processing** in order to image the geological structures.

2 FIELD DATA ACQUISITION PARTICULARS

2.1 Time Schedule and Region's Information

At 20 SED earthquake monitoring stations in the Swiss Alps, the Prealps, the Foreland Basin and the Jura Range, seismic surveys have been done to obtain the seismic shear wave velocities.

Survey No.	Name	Canton	Region	Geological Unit	Date of Fieldwork	# profiles P*	S*	M*
1	ACB	AG	Jura	Tabled Jura	03.03.09	2	2	2
2	AIGLE	VD	Prealps	Penninikum	07.04.09	2	2	2
3	BALST	So	Jura	Folded Jura	06.05.09	2	2	2
4	BNALP	NW	Alps	Helvetikum	10.06.09	2	2	2
5	BOURR	JU	Jura	Folded Jura	18.12.08	1	1	1
6	BRANT	NE	Jura	Folded Jura	19.05.09	2	2	2
7	FLACH	SH	Foreland	OMM/USM	03.02.09	2	1	2
8	GIMEL	VD	Jura	Folded Jura	18.05.09	2	2	2
9	HASLI	BE	Alps	Helvetikum	23.04.09	2	2	2
10	LLS	GL	Alps	Parautochthon	30.03.09	1	1	1
11	MUO	SZ	Alps	Helvetikum	18.06.09	2	2	2
12	PLONS	SG	Alps	Helvetikum	14.05.09	2	2	2
13	SKEH	OW	Alps	Helvetikum	20.03.09	2	2	2
14	SLE	SH	Jura	Tabled Jura	11.12.08	1	1	1
15	STEIN	SH	Foreland	OSM	07.05.09	2	2	2
16	SULZ	AG	Jura	Tabled Jura	15.12.08	2	1	2
17	TORNY	FR	Foreland	Quaternary/OMM	06.04.09	2	2	2
18	WEIN	TG	Foreland	Quaternary/OSM	04.03.09	2	2	2
19	WILA	ZH	Foreland	OSM	15.04.09	2	2	2
20	WIMIS	BE	Prealps	Penninikum	24.04.09	2	2	2

* P: p-wave refraction/reflection survey; S: s-wave refraction/reflection survey; M: MASW survey.

Tab. 2.1 Summary information about the SED Station positioning and the seismic surveys.

Fig. 2.1: S-wave data acquisition at SED station WIMIS. In front of the motorized wheel-barrow the seismic shear wave source with steely spikes for fixation at ground.

2.2 Summary of Data Acquisition Parameters

2.2.1 Compressional wave data acquisition

# of active channels	96
geophone type	4.5 Hz natural frequency, vertical velocimeter
receiver station spacing	mainly 1.0 m; @ LLS & WIMIS: 1.5 m
# of geophones/station	1
source point spacing	2.0 m to 3.0 m
source type	vertical hammer (8 kg) striking on a horizontal metal plate
sampling rate	500 µs
recording time	2048 ms
field filters	0.5 Hz LC, anti-alias
# of field records / profile	~ 48

2.2.2 Shear wave data acquisition

# of active channels	48
geophone type	10 Hz natural frequency, horizontal velocimeter
receiver station spacing	mainly 2.0 m; @ LLS & WIMIS: 3.0 m
# of geophones/station	1
source point spacing	4.0 m to 6.0 m
source type	mainly horizontal hammer (8 kg) striking horizontally at a metal-plated wooden beam anchored to the ground by means of 20 cm long spikes @ LLS & WIMIS: horizontal strike against solid rock
sampling rate	500 µs
recording time	512 ms
field filters	2 Hz LC, anti-alias
# of field records / profile	~ 48

Fig. 2.2: Man-powered p-wave data acquisition at SED station TORNY striking the metal plate (left in the pasture) with the 8 kg hammer. The backpack contains the radio link for trigger signal.

2.3 Composition of Seismic Field Crew

2.3.1 Personnel

Lorenz Keller	dipl. sc. nat. ETHZ, geophysicist; party chief
Walter Frei	dipl. sc. nat. ETHZ, geophysicist; party chief
Jochen Fiseli	dipl. sc. geol., University of Freiburg i. Br., geologist, party chief
Philippe Corboz	dipl. sc. nat. ETHZ, geophysicist, party chief.
Dieter Martin	dipl. sc. geol., University of Freiburg i. Br., geologist, observer, assistant
Kieron Lynch	assistant, spread lay-out and activation of seismic source
Fabian Isler	assistant, spread lay-out and activation of seismic source
Christoph Brander	assistant, spread lay-out and activation of seismic source
Volker Fink	assistant, spread lay-out and activation of seismic source

2.3.2 Equipment

96	vertical geophones 4.5 Hz
48	horizontal geophones 12 Hz
6	seismic cables
1	seismic acquisition system Summit Compact, 96 channels
1	laptop computer for data acquisition
3	walkie-talkies
1	hammer 8 kg
1	steel plate
1	metal-plated wooden beam
1	motorized wheel barrow
1	van (FIAT Ducato 4x4)

Fig. 2.3: Improvisational seismic data registration in the gallery at SED station LLS. The yellow boxes in the foreground contains 24 channel A/D converter each. The sensors (yellow case in the middle foreground) are firmly plugged in small holes drilled into the concrete foundation of the gallery's bottom. In the background the cabinets with the earthquake monitoring station instrumentation.

2.4 Location

The 20 earthquake monitoring stations are spread all over Switzerland, north of the alpine main ridge. 7 surveys were carried out in the Jura range, 5 in the sediments of the foreland basin, 3 in the prealps and 3 in the alps.

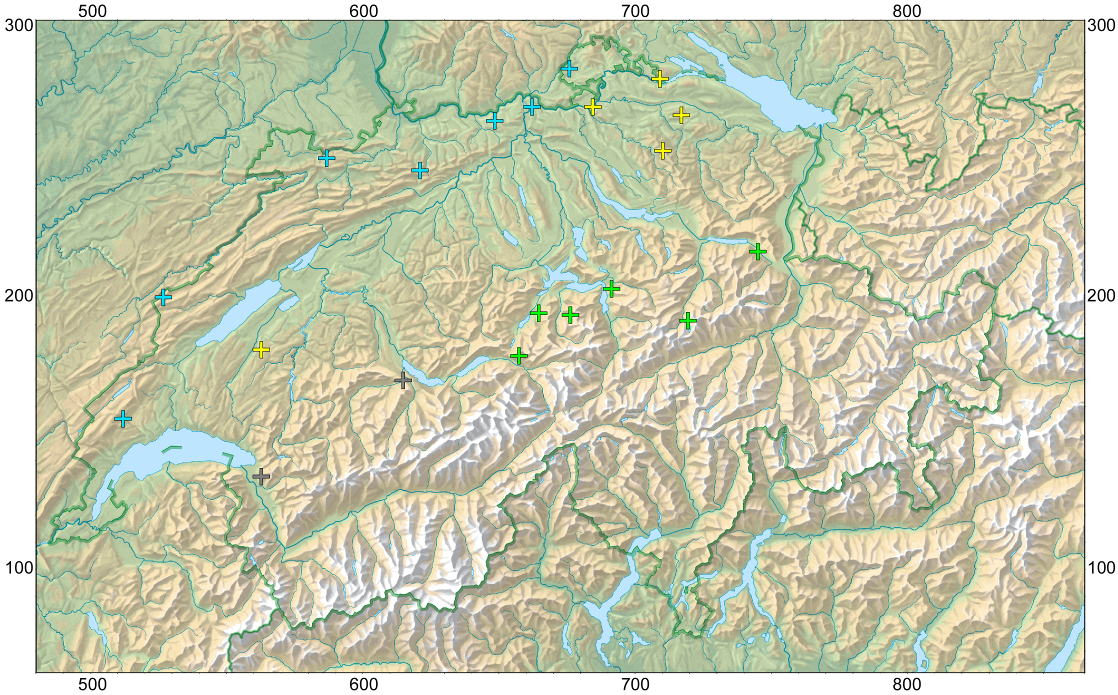

Fig. 2.4: The red crosses mark the 20 seismic monitoring stations. In blue: Jura range; in yellow: foreland basin; in gray: prealps (Penninikum); in green: alps (mostly Helvetikum). (map: geodata @ swisstopo).

Fig. 2.5: S-wave source transportation along the seismic profile at SED station AIGLE.

2.5 Recording Conditions and Line Setup

No.	Name	Weather conditions	Observed noise	Seismic data quality	Remark
1	ACB	cold, drizzle	-	fair – good	-
2	AIGLE	warm, dry	construction work	fair	-
3	BALST	warm, dry	unknown source*	good	karstified geology
4	BNALP	warm, dry	-	good	rough terrain*
5	BOURR	frozen, 30 cm snow	-	fair – good	-
6	BRANT	warm, dry	-	excellent	above cave?*
7	FLACH	warm, dry	-	good	rough terrain*
8	GIMEL	warm, dry	-	good	-
9	HASLI	cold, dry, partly snow	air traffic*	fair – good	rough terrain*
10	LLS	-	-	good	in gallery
11	MUO	warm, dry	air traffic*	good	above galleries
12	PLONS	warm, dry	-	good	complex geology*
13	SKEH	cold, dry, windy	construction work	deficient – fair	nearest to buildings
14	SLE	frozen, 20 cm snow	-	good	-
15	STEIN	warm, dry	mowing work*	fair – good	complex geology
16	SULZ	frozen, 20 cm snow	-	good – excellent	-
17	TORNY	warm, dry	-	excellent	-
18	WEIN	cold, drizzle	-	good	rough terrain*
19	WILA	warm, dry	-	good – excellent	rough terrain*
20	WIMIS	warm, dry	-	fair – good	-

* only on one single profile

Tab. 2.2: Conditions and seismic data quality of all surveys.

Fig. 2.6: Geophone lay-out and monitoring car at SED station SULZ.

3 SEISMIC DATA PROCESSING AND IMAGING OF THE RESULTS

3.1 General Remarks

3.1.1 Software

- For the shear and compressional wave refraction seismic evaluation the packages RAY-FRACT by Intelligent Resources Ltd., Vancouver CAN, was used. The system features the technique of diving wave tomography (www.rayfract.com).
- The system **SPW** (**S**eismic **P**rocessing **W**orkshop) of Parallel Geoscience Corporation, Austin US-TX, was used for reflection seismic data processing (www.parallelgeo.com).
- Data processing of surface waves (MASW processing) was conducted with the software package **SurfSeis** V2.0 of Kansas Geological Survey in Lawrence US-KS.

3.1.2 Personnel

Lorenz Keller, dipl. sc. nat. ETHZ, geophysicist	MASW, refraction & reflection seismics, interpretation
Jochen Fiseli, dipl. sc. geol. Univ. Freiburg i.Br.	refraction & reflection seismics
Philippe Corboz, dipl. sc. nat. ETHZ, geophysicist	refraction & reflection seismics

3.1.3 About detailed results of each survey

Please refer to the respective station reports in appendices for detailed information about field observations, results and interpretations.

The following description of processing steps gives an overview of processing history illustrated by the data set of line 09SN_17TORNY-1.

3.2 MASW Processing

3.2.1 Data conditioning

The data preparation steps for the dispersion analysis include

- the assignment of the field acquisition geometry
- the selection of suitable offset ranges (=arrays) for dispersion analyzes, and the splitting of the field records in forward and reverse shooting direction data sets
- the reformatting of the data into the specific KGS format

X - - ... - - o-o-o-...-o-o-o (forward shooting or so-called PLUS direction)
respectively
o-o-o-...-o-o-o - - ... - - X (reverse shooting or so-called MINUS direction).

where **X** = shot position
o = receiver station
- = 1.0 m offset

The active array used for MASW analyzes normally spread over 10 to 50 m shot-receiver offset and one all-over array for each direction and profile.

In some rare cases, the seismic data are muted, i.e. top mute (to blank refraction events) or surgical mute (aerial noise from external sources)

3.2.2 Dispersion analysis

3.2.2.1 Calculation of dispersion image

The dispersion of surface waves describes the correlation between frequency and the respective phase velocity. The algorithm is based on a wavefield transformation from offset-time (x,t) domain into phase velocity-frequency (C_f-f) domain (Park et al., 1999). For each array – as well of both profiles as of both processing directions – containing maximal traces in the offset selection the dispersion is computed. The result of dispersion analysis is the color encoded acoustic energy distribution in the phase velocity - frequency plane (see Fig. 3.3a).

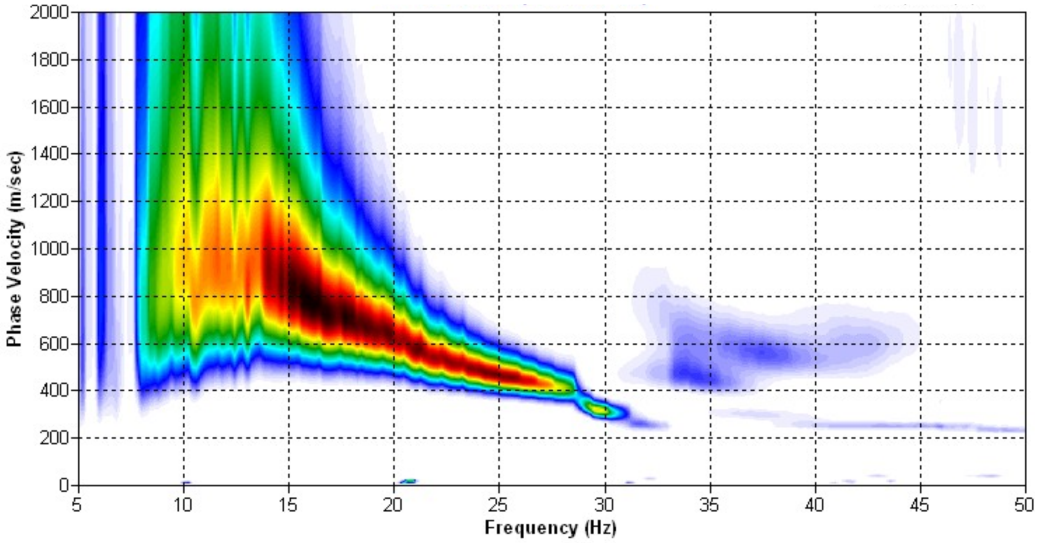

Fig. 3.2a: Dispersion image as the result of dispersion analysis of an 40-m-array. horizontal axis: frequency [Hz]; vertical axis: phase velocity; color code: amplitude of dispersion [%], from white = 0% over blue = 20%, green = 50%, yellow = 70 % and red = 80 % to black = 100 %.

3.2.2.2 Analysis of the dispersion image

In the dispersion image as calculated in section 3.3.2 above, the curves joining the amplitude peaks of the fundamental modes are determined either by subjective inspection or in a semi-automated manner.

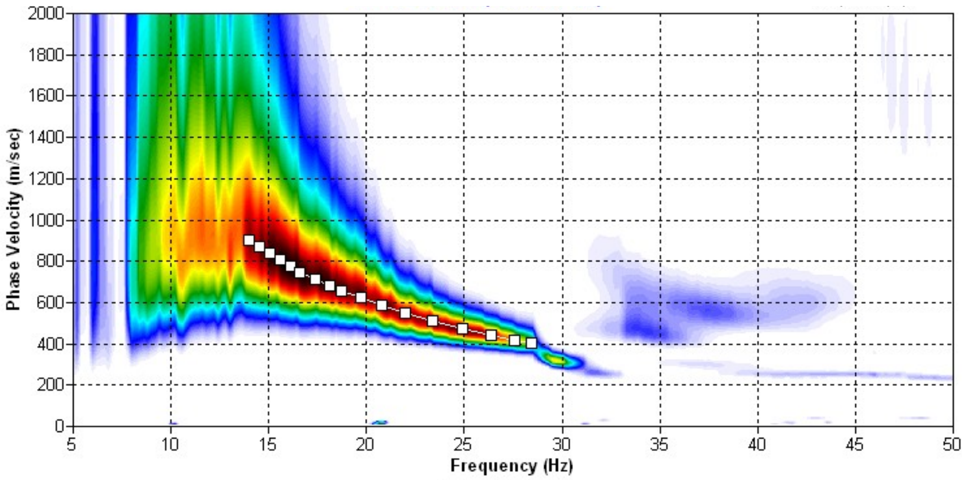

Fig. 3.2b: The manually picked dispersion images used for the derivation of the shear wave velocity section. The dispersion curves (white squares) are determined by linking the peaks of high energy. Red line: high resolution beam-forming curve for v_{max}.

3.2.3 Inversion process

3.2.3.1 Calculation of starting model

An initial velocity model is computed by analyzing a high quality dispersion curve. Generally, a 10 layer model with continuously increasing layer thicknesses, made up of 9 layers down to the maximum depth (z_{max}) to be in the order of 30% of the largest wavelength. That layer model frames the initial model for each inversion (see 3.3.3.2), the respective velocities are computed for each dispersion model. For all 10 layers the Poisson's ratio is normally assumed to be 0.4 and the rock/soil density to be 2.0 g/cm^3.

In some cases, where the observed dispersion is extremely low, the velocity of half space layer is changed manually to a more realistic – namely of the same size like the 9 layer above – velocity.

3.2.3.2 Inversion of dispersion curves resulting in a 1D shear wave velocity distribution

The iterative inversion process is concluded either after 12 iterations or when the convergence condition of a RMS-error of less than 5 % (phase velocity) is met. For calculation details of inversion we refer to Xia et al. (1999).

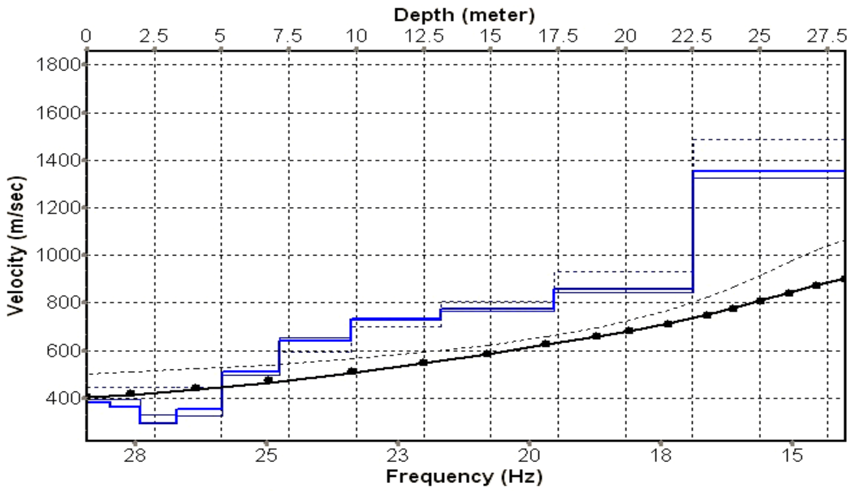

Fig. 3.2c: Inversion results of dispersion curve.
brown: Inversion of dispersion curve (dots) resp. of the modeled dispersion curve (dotted line: initial model; continuous line: end model). Horizontal axis: frequency Hz, vertical axis: vs.
blue: 10-layer-model (dotted: initial model, continuous fine line: second last model; continuous thick line: final model). Horizontal axis: depth [m] resp. frequency [Hz], vertical axis: phase velocity [m/s]).

3.2.4 Results from MASW analysis

3.2.4.1 *Gridding and plotting of 2D v_s-velocity field*

By assembling the 1D v_S - depth functions of all stations the final 2D v_S-field is derived using a Kriging gridding procedure as portrayed in Fig. 3.3h and 3.3i below:

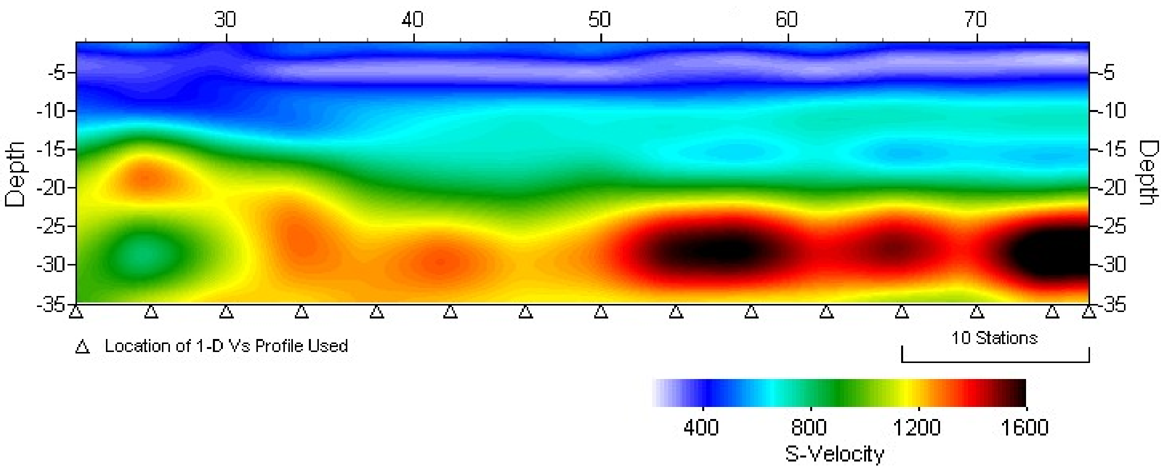

Fig. 3.2d: MASW-processed shear wave velocity fields as result of the inversion processing.

3.2.4.2 *Tabular data of velocities*

In discussion of the derived results (refraction and MASW velocities) with an expert (Dr. D. Fäh, Swiss Seismological Service) and a representative of the client (Dr. Ph. Renault), a section of the seismic profile was selected to calculate a mean velocity model representing the geological setting at the earthquake monitoring station.

Depth [m]	Vs+ [m/s]	Vs- [m/s]	Vs [m/s]
1.0	400	397	399
2.2	182	212	197
3.8	441	425	433
5.8	544	578	561
8.2	578	604	591
11.2	722	764	743
15.1	883	998	941
19.8	1060	1162	1111
25.8	1111	1177	1144
32.2	1274	1256	1265

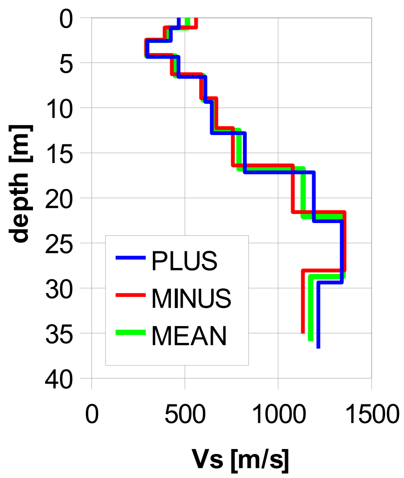

Tab. 3.2a: Averaged v_S-depth function representing the SED station.
Blue line: MASW-'PLUS' processing, red line: MASW-'MINUS' processing;
green line: average of PLUS- and MINUS-functions.

A comparison of all derived mean shear wave velocity models of each line and direction gives a good overview of results quality (Tab. 3.2b and Fig. 3.2e).

	100 m array							40 m array					
depth	m1+	m1-	m2+	m2-	m1	m2	m	depth	m1	depth	m2	depth	m
1.6	452	491	545	438	471	463	496	1.1	514	1.0	399	1.1	456
3.5	743	486	247	381	614	243	492	2.5	408	2.2	197	2.4	302
5.9	290	460	896	239	375	746	548	4.2	296	3.8	433	4.0	364
8.9	849	592	577	476	720	633	672	6.4	448	5.8	561	6.1	505
12.7	932	753	872	597	843	847	852	9.1	599	8.2	591	8.7	595
17.5	737	878	1001	689	808	1002	872	12.5	656	11.2	743	11.9	700
23.4	943	999	1280	821	971	1256	1074	16.8	789	15.1	941	15.9	865
30.8	1346	1183	1430	905	1264	1430	1320	22.1	1134	19.8	1111	21.0	1122
40.0	1629	1435	1689	1004	1532	1689	1585	28.7	1348	25.8	1144	27.2	1246
50.0	2535	2372	1727	1232	2454	1727	2211	35.9	1174	32.2	1265	34.1	1220

Tab. 3.2b: vs-depth values of all MASW inversions at SED station.

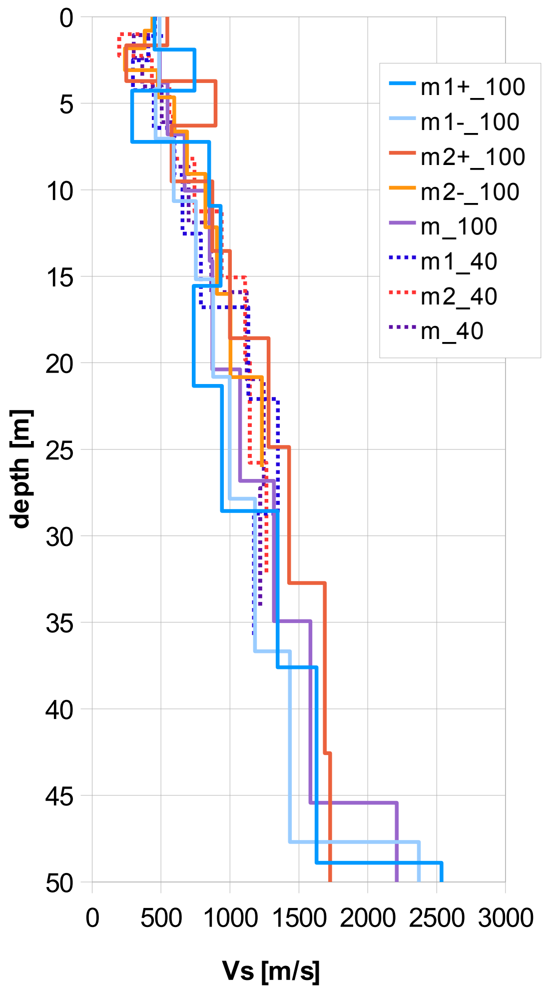

Fig. 3.2e: Comparison of the ensemble of inversion results of both lines and both directions at SED station, each using the 40-m- and the 100-m-arrays.
blue lines: analyzes of records of line 1
red lines: analyzes of records of line 2
magenta line: mean of both lines and both directions for 100-m-array resp. 40-m-array.
continuous lines: models of 100-m-array analyzes
dotted lines: models 40-m-array analyzes.

3.2.5 Calculation of the shear wave velocity scalars $v_{s,5}$, $v_{s,10}$, ...

The parameters $v_{s,5}$, $v_{s,10}$, $v_{s,20}$, $v_{s,30}$, $v_{s,40}$, $v_{s,50}$ represent the average shear wave velocities in the depth interval between the surface and the respective depth levels and are determined from the formula

$$v_{s,n} = \frac{\sum_{i=1}^{n} d_i}{\sum_{i=1}^{n} d_i / v_{si}}$$

with:

d_i = thickness of layer i
v_{si} = corresponding shear-wave velocity.

The derived $v_{s,5}$, $v_{s,10}$, ... distributions are plotted in Fig. 3.2f.

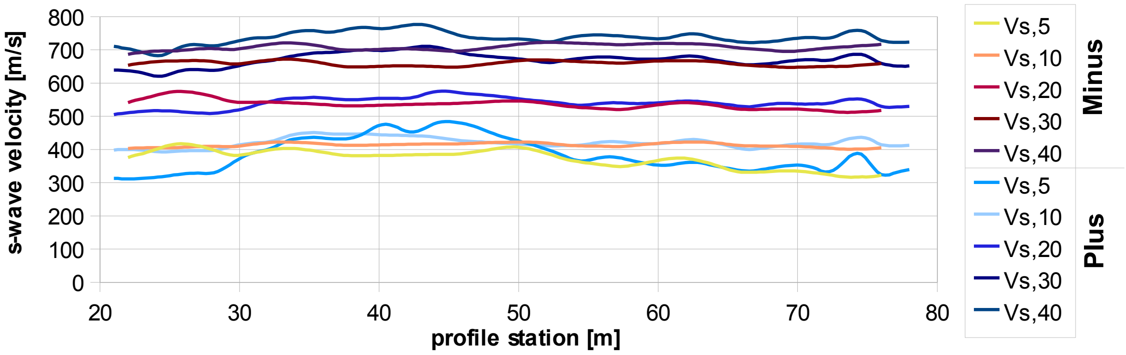

Fig. 3.2f: Graphs of the averaged $v_{s,5}$...-values along the seismic line for the PLUS- (blue lines) and MINUS- (red lines) direction.

The average values of the s-wave velocity model $v_{s,5}$, $v_{s,10}$, $v_{s,20}$, $v_{s,30}$, $v_{s,40}$, $v_{s,50}$, $v_{s,100}$ (= average shear wave velocity from the surface to depths of 5 m, … until 40 m) on the line segment nearest to the SED station (Tab. 3.3d) are summarized below:

	Vs,5	Vs,10	Vs,20	Vs,30	Vs,40
MINUS	373	413	536	659	708
PLUS	384	421	541	671	737
MEAN	378	417	538	665	722

Tab. 3.2c: The average shear wave velocities within the depth intervals from surface down to 5 m, etc.… to 40 m, calculated for the whole line.

3.3 Seismic Refraction Tomography

3.3.1 Data conditioning

3.3.1.1 Reformatting and quality verification of field data and gain recovery

The field format SEG2 is being converted to the internal format of the Rayfract or ReflexW (shear wave data) resp. SPW processing system. The dynamic automatic gain and the pre-amplifier gain applied in the field are inversely applied to the seismic data in order to restore true amplitude data. Validation of the completeness, and assessment of the quality of the data set.

3.3.1.2 Recording geometry assignment

The recording geometry and the topographical survey information (x, y, z – station coordinates) are assigned to the seismic data.

3.3.1.3 Data editing (suppression of bad / dead traces, etc.)

Checking the correctness of the line geometry assignment; suppression of dead and bad traces, spectral analysis of the data at various offsets.

3.3.1.4 Preliminary analysis of refraction velocities

First seismic event arrival time analysis to get a first view of rock velocities.

3.3.2 First break time picking

3.3.2.1 Picking the compressional wave data

At each seismic trace in each record, the first event identified as compressional wave – this is normally the first seismic event, except in cases, where the sonic noise of source is faster than the direct wave in soil – is manually set by time marks. Traces with low S/N level are filtered carefully and in some cases excluded from FB time picking.

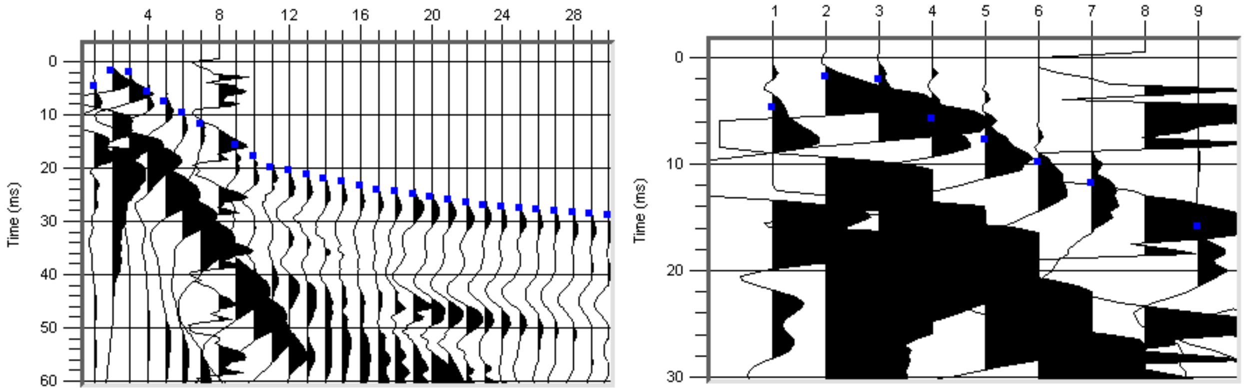

Fig. 3.3a: p-wave record (left) and detail of source (right) around the source (shot position 2.5) with positive amplitude excursions in black. Receiver 8 is a dead trace. Blue squares mark the manually picked first break arrival times. The detail shows that the first events on the seismic traces are of air wave (source triggered noise) and do not represent the direct soil wave.

3.3.2.2 *Picking the shear wave data*

At each shot position, two seismic records were acquired in both activation directions. These two records are displayed superimposed with different colors on each other. The seismic shear wave first break time is normally defined by the change of polarization (opposed amplitudes, see Fig. 3.3b). In some cases when the polarization is not well formed, a second characteristic of shear wave is drawn: larger amplitudes and lower frequencies, an event approx. two times later than the p-wave first break.

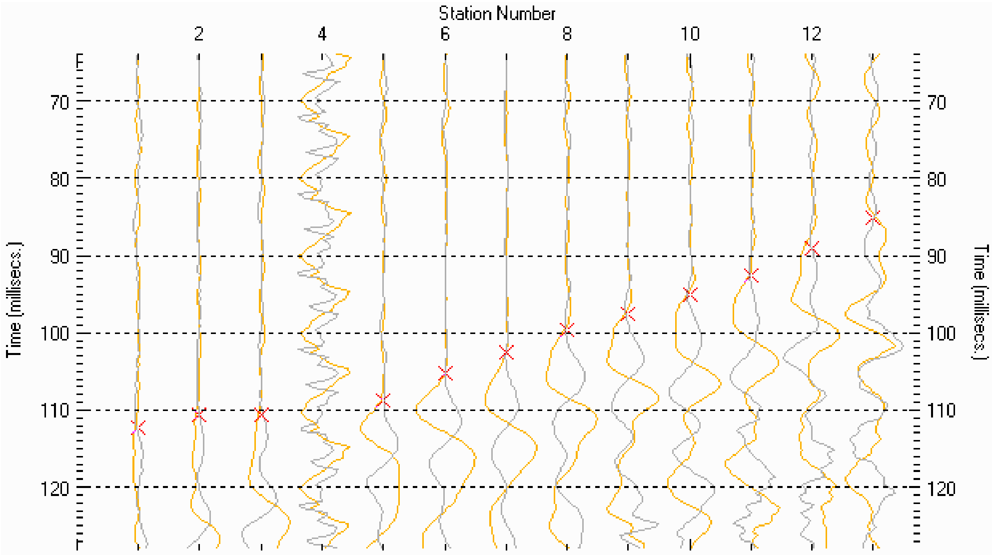

Fig. 3.3b: A detail from a high quality dual field record showing at each station the s-wave traces with opposing polarities in yellow and gray colors. Receiver 4 is a dead trace. The manually picked s-wave refraction arrivals at each station are marked with a red x.

3.3.2.3 *Quality control of first break times picks*

All first break times are displayed and controlled regarding consistency between records (see Fig. 3.3c)

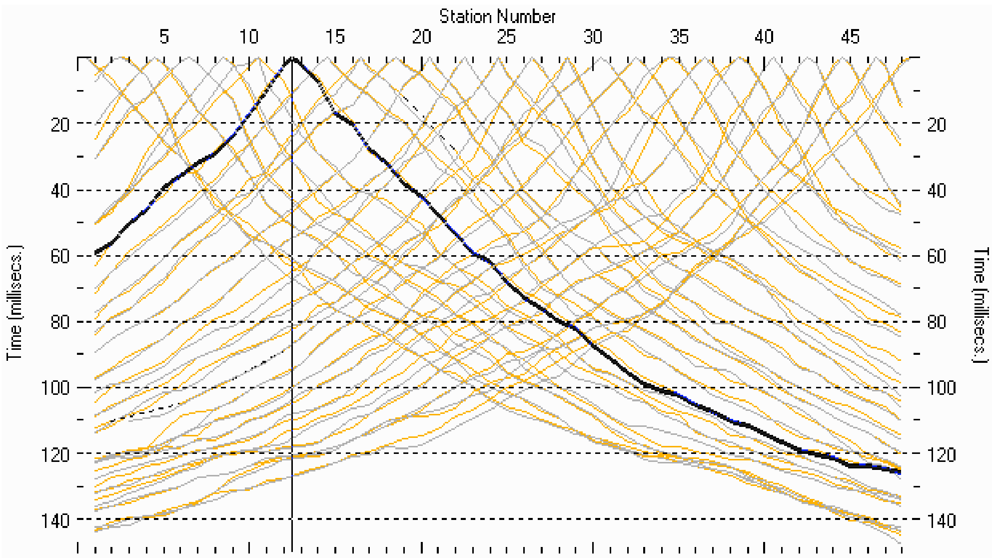

Fig. 3.3c: Display of all s-wave first break time curves of seismic line for quality control purposes. The colors respond to the two directions of stimulation as in Fig. 3.3b.

3.3.3 Analytical Determination of Initial Refraction Velocity Model

An initial 1D-velocity function is computed by averaging velocity-depth profiles derived by the *Delta-t-V method* (Gebrande and Miller, 1985 and Gebrande, 1986), so called *gradient method*. In some cases of good layered geology and flat topography, the initial velocity model derived by Delta-t-V could be used as initial model for inversion. The initial velocity model is determined in the 3-dimensional time-offset-CMP-domain of all first break arrival time curves in the 3-dimensional time-offset-CMP-domain (see. Fig. 3.3d).

3.3.3.1 CMP sorting

All first break times are sorted in the 3-dimensional coordinate system defined by the x-axis (CMP-position), the travel time axis and the source-receiver-offset axis (see. Fig. 3.3d).

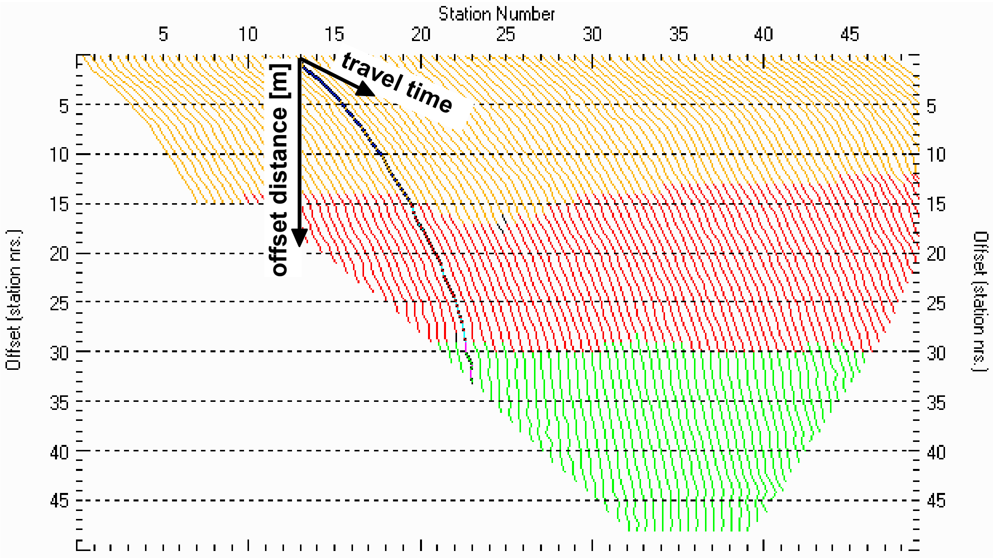

Fig. 3.3d: 3-dimensional distance-travel time diagrams at the mid-points between source points and receiver stations are instrumental when using the analytical CMP derivation of the initial velocity field.
The horizontal axes are along the CMP positions and the travel time respectively, the vertical axis denotes the offset distance between source and receiver positions. The colors represent different velocity layers.

3.3.3.2 Velocity determination

The initial velocity model is determined by temporal derivative of offsets in the CMP domain received by previous step in specific time- and station steps. Depending on the chosen method, this velocity field is averaged along the profile axis (1D-gradient method) resp. left as it is (Delta-t-V-method).

3.3.3.3 Gridding

To prepare the velocity field for the following inversion, it is gridded to a regular grid using the Kriging method.

3.3.4 Tomographic inversion of the velocity gradient field by iterative modeling

The velocity field is iteratively refined by the subsequent Wavepath Eikonal Traveltime (WET; Schuster 1993; Watanabe 1999) tomographic inversion process. For a successful inversion, normally 20 to 100 iteration steps are computed, depending on topographic variations and subsurface heterogeneity.

3.3.5 Results from refraction velocity determination

3.3.5.1 Images of velocity distribution

The inversion results are portrayed in Fig. 3.3e as a gridded velocity contour section and in Fig. 3.3f as a ray path density section.

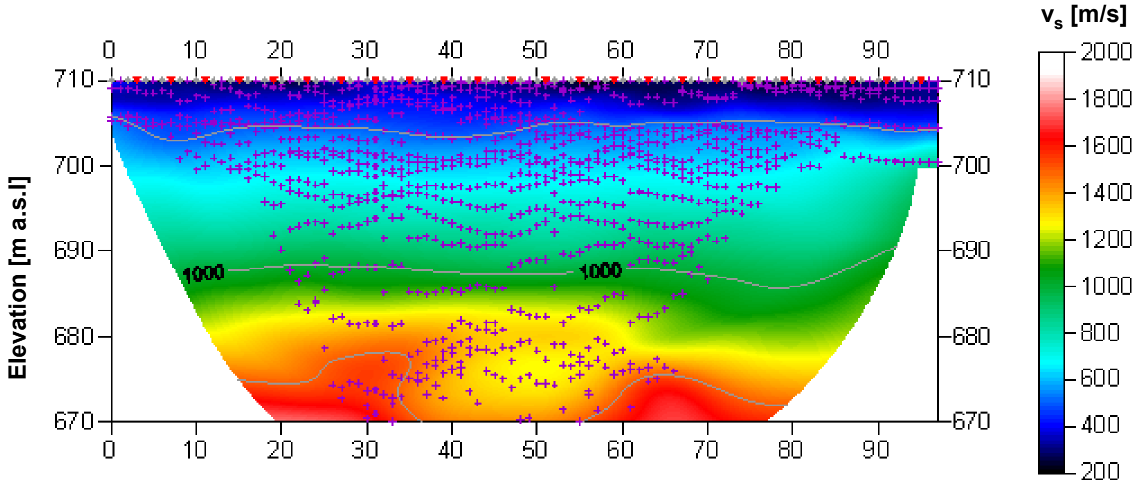

Fig. 3.3e: Shear wave velocity field of the line. Red/white colors denote solid rock, blue/black colors point to unconsolidated sediments and soil.

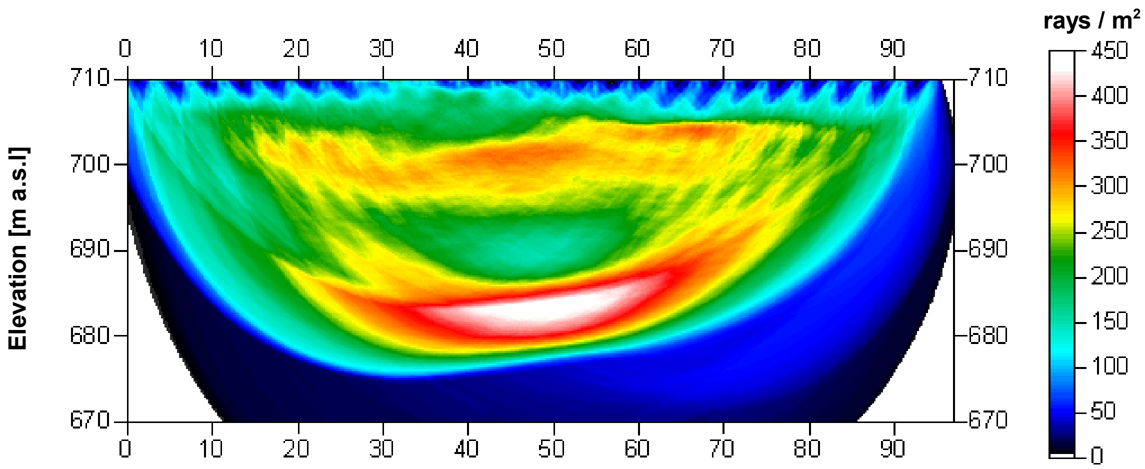

Fig. 3.3f: Shear wave ray path density along the seismic line. Red/white colors indicate high velocity contrasts (usually at the bedrock surface), blue/black colors denote low coverage areas.

3.3.5.2 Tabular data of velocities

In discussion of the derived results (refraction and MASW velocities) with an expert (Dr. D. Fäh, Swiss Seismological Service) and a representative of the client (Dr. Ph. Renault), a section of the seismic profile was selected to calculate a mean velocity model representing the geological setting at the earthquake monitoring station.

The velocity field values (elevations) are converted to depth and subsequently computed as non-weighted averages over the selected portion.

Depth [m]	Vs [m/s]
0.0	394
2.8	269
5.7	492
8.5	741
11.3	902
14.0	941
16.8	955
19.7	970
22.5	1016
25.3	1097
28.0	1184
30.8	1237
33.6	1303
36.5	1378
39.3	1435
42.0	1495

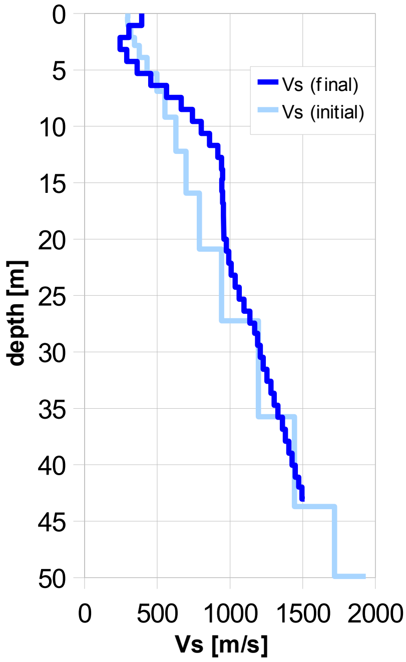

Tab. 3.3: Final 1D s-wave velocity model derived from real data (horizontal average of all values) representing the situation at the earthquake monitoring station.

3.4 Reflection Seismic Data Processing

The following description of seismic processing steps gives an overview of the potentially applied processing sequence. Depending on survey's conditions, some of theses steps are canceled.

3.4.1 Data conditioning

3.4.1.1 Reformatting and quality verification of field data and gain recovery

The field format SEG2 is being converted to the internal format of the SPW processing system. The dynamic automatic gain and the pre-amplifier gain applied in the field are inversely applied to the seismic data in order to restore true amplitude data. Validation of the completeness, and assessment of the quality of the data set.

3.4.1.2 Recording geometry assignment

The recording geometry and the topographical survey information (x, y, z – station coordinates) are assigned to the seismic data.

3.4.1.3 Data editing (suppression of bad / dead traces, etc.)

Checking the correctness of the line geometry assignment; suppression of dead and bad traces, spectral analysis of the data at various offsets.

3.4.1.4 Preliminary analysis of refraction velocities

First seismic event arrival time analysis to get a first view of rock velocities.

3.4.2 Filtering and deconvolution

3.4.2.1 Analytical muting of refraction arrivals

In order to prevent excessive NMO stretching to shallow data and from larger offsets, and also to prevent the stacking of refracted arrivals, an offset dependent mute zone is defined at regular intervals along the seismic profiles. Within this mute zones the data are zeroed by using a Hanning type taper window at the mute zone boundaries.

3.4.2.2 Amplitude equalization in time and frequency domains

Application of time-variant amplitude scaling for compensation of attenuation loss with increasing depth and increasing offsets. An instantaneous **A**utomatic **G**ain **C**ontrol (AGC) function is applied using RMS amplitude scaling windows of variable lengths starting with 50 ms at the top of the record (0 ms TWT) and increasing linearly to 200 ms at 500 ms TWT.

3.4.2.3 Predictive deconvolution parameter tests / application

Since the survey may be affected by a considerable ground unrest with a predominant frequency of 16 $^{2}/_{3}$ Hz (railway) and/or 50 Hz (power supply) a gapped deconvolution procedure is applied for suppressing this noise.

3.4.2.4 Determination of band limiting corner frequencies / band-pass-filter application

The frequency band limiting filter is applied to attenuate low frequent high ground roll energy and to eliminate acoustic noise and/or ground unrest originate not from subsurface source reflections.

3.4.2.5 Optional 2-D filtering

Frequency – wavenumber (f-k) band limiting filter. This filter is applied to attenuate linear noise such as source generated noise, air traffic and – restricted – ground groll.

3.4.3 Velocity analysis and stack

3.4.3.1 Common Depth Point (CDP) sort

The data are sorted in the **C**ommon **D**epth **P**oint (CDP) domain to get information belonging the same geological setting.

3.4.3.2 Semblance velocity analysis using supergathers

At regular intervals along the profiles groups of several CDP gathers are combined into CDP supergathers for semblance velocity analysis.

3.4.3.3 Normal Move-Out (NMO) correction and application of stretch mute

Normal **M**ove **O**ut correction; i.e. travel time and offset dependent arrival time correction which horizontally aligns reflection events of all source – receiver traces at a particular CDP-position. Data affected by more than 30% NMO stretching are muted.

3.4.3.4 Optional dip move-out (DMO) correction

The multichannel operation **D**ip **M**ove **O**ut (DMO) correction shifts arrival times to all possible positions – they are located along an elliptic shape – where the source – reflection point – receiver-offset are of the same length.

3.4.3.5 Automatic surface consistent residual statics (horizon guided sliding design windows)

Procedure to better align NMO corrected traces within a CDP gather. A small number of prominent horizon events, as identified on a previously created brute stack, are assigned to not more than two derive windows for calculating residual time shift corrections. The time shifts thus obtained are the result of a analysis of arrival time variations caused by velocity and elevation variations at the source and receiver positions. The derive windows are dynamic in length as well as in time in order to account for depth variations along the chosen reflection horizon events.

3.4.3.6 Sub-surface consistent trim residual static corrections

A mathematical attempt to still better align the traces in a CDP-gather. The traces are correlated with a pilot reference trace iteratively derived usually by a summation of all or a limited number neighboring traces.

3.4.3.7 Band-pass filtering

This filter is applied to enhance the visibility of reflection events and for shaping the signal spectrum for obtaining a higher resolution.

3.4.3.8 CDP stack

Signed traces over all offsets or in a specific offset range are summed horizontally, resulting in a single stacked trace at each CDP position.

3.4.3.9 Optional coherency filtering (by f-x deconvolution)

A cosmetic procedure to improve the lateral continuity of reflection events.

3.4.4 Stack finalizing and time-depth conversion

3.4.4.1 Optional spiking deconvolution

Processing step to reduce multiple reflections between two overlying horizons (i.e. ringing).

3.4.4.2 Band-pass filtering

This frequency band limiting filter is applied to enhance the visibility of high frequent events.

3.4.4.3 Trace amplitude balancing with sliding window AGC

Scaling for attenuating high amplitude values in the near surface domain. An instantaneous **A**utomatic **G**ain **C**ontrol (AGC) function is applied using RMS amplitude scaling windows of linearly increasing lengths.

3.4.4.4 Depth conversion

Using the velocity functions derived by refraction tomography and by semblance velocity analysis for converting TWT sections into depth sections by taking into account the relief elevations of the surface.

3.4.4.5 Final display of seismic depth section with inverse polarity (non-SEG-convention)

Display of the data with reversed polarity. As opposed to the SEG convention, the compressional phase of a reflection event is displayed as a positive amplitude excursion, i.e. in black.

3.4.5 The presentation of reflection seismic data

The data in a reflection seismic section are presented as an assembly of individual seismic signals at regular intervals along a seismic profile. The simplest way of representing the signals are single wiggle lines (first to the left in the illustration below). A more capturing presentation is the variable area form (second to the left). Combining these two modes results in the var-wiggle mode. Another method of data visualization is the variable density mode (second from the right).

The compressional phase of seismic signals is defined in this report as the onset of the positive amplitude excursion in black (Fig. 3.4a). Since the source signal is produced by an explosion or by an impact at the surface, the signal starts off with a compression of the ground particles. Thus the arrivals of reflection events are defined by the compressional phase.

In rare situations of velocity inversions, cases in which formation velocities are lower than in the layers above, polarity reversals of the reflected signals occur. The beginning of the reflection event would then be characterized by a dilatational phase, represented in this report as a negative amplitude excursion, i.e. in white.

The final p-wave seismic depth sections are displayed in Fig. 3.4b, the hybrid sections in Fig. 3.4c and d.

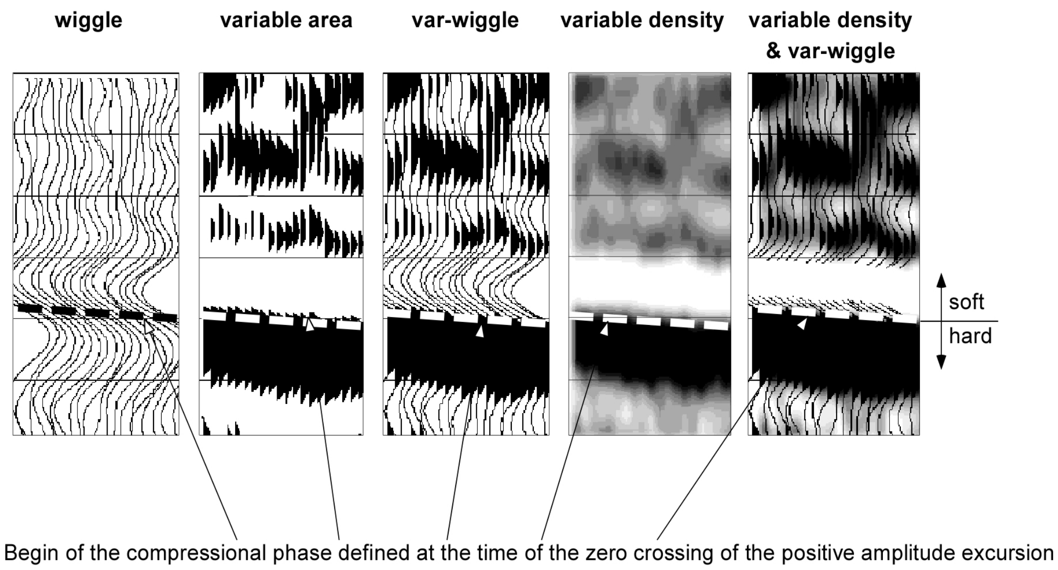

Fig. 3.4a Representation of reflection seismic data and the definition of a reflection event.

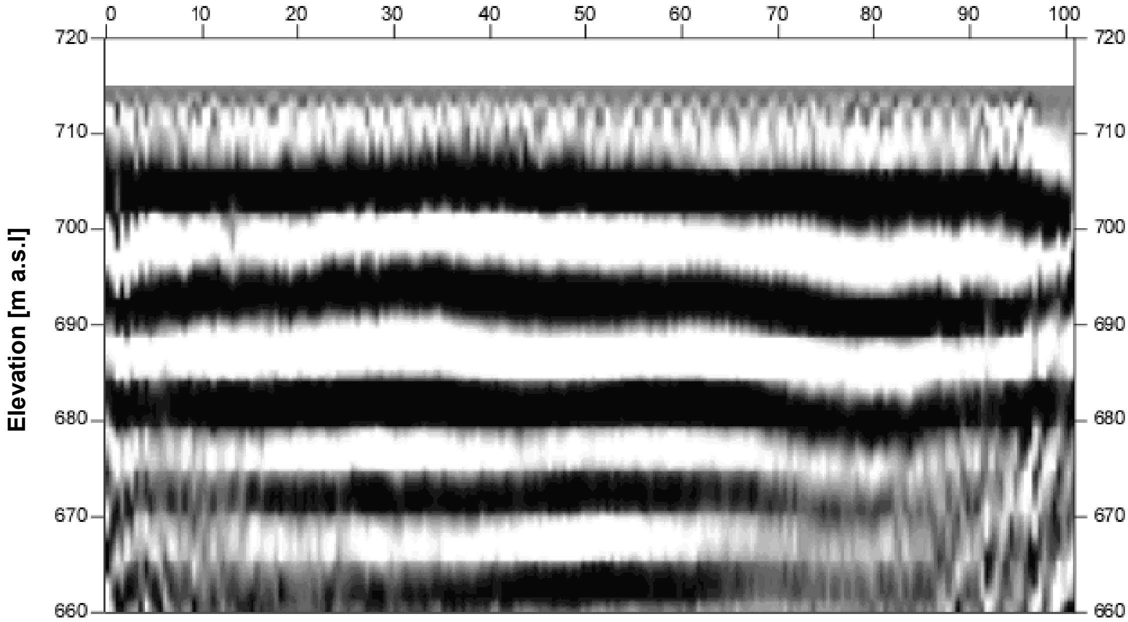

Fig. 3.4b: Display of seismic p-wave depth section with variable density mode presentation.

3.4.6 Representation of the hybrid seismic section

The hybrid seismic section is the reflection seismic section with the superimposed p-wave velocity field. It portrays the geological structures and the p-wave velocity field, the latter being indicative for the rock / soil rigidity. The uninterpreted hybrid seismic section is portrayed in Fig. 3.4j and 3.4k below.

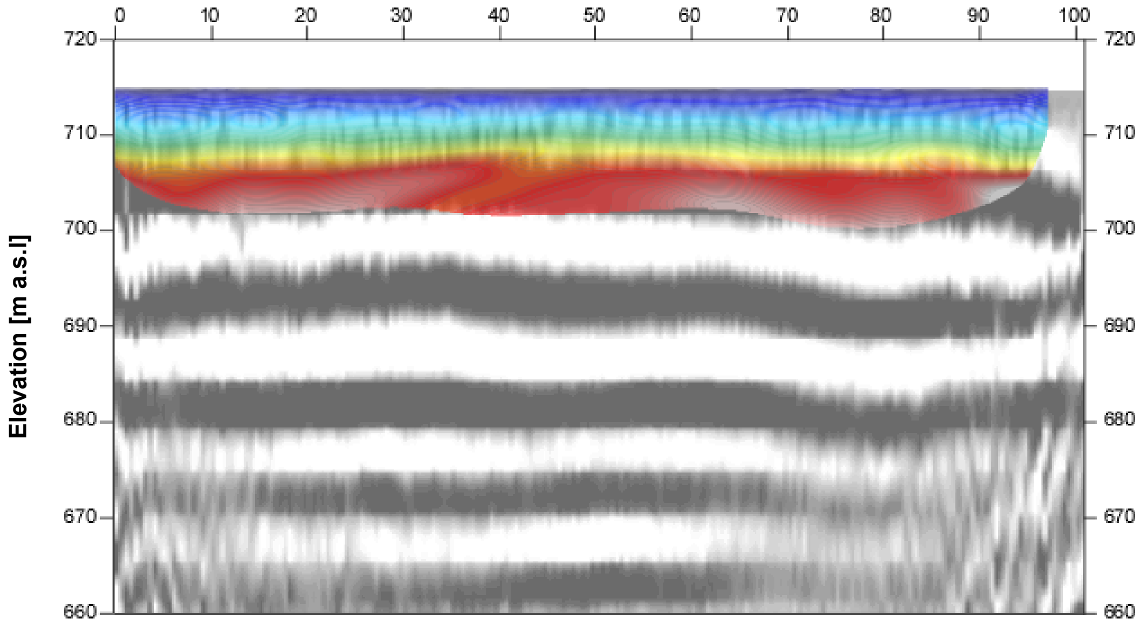

Fig. 3.4c Uninterpreted hybrid seismic section: superimposed onto the seismic reflection section is the color encoded p-velocity field derived by refraction tomography.

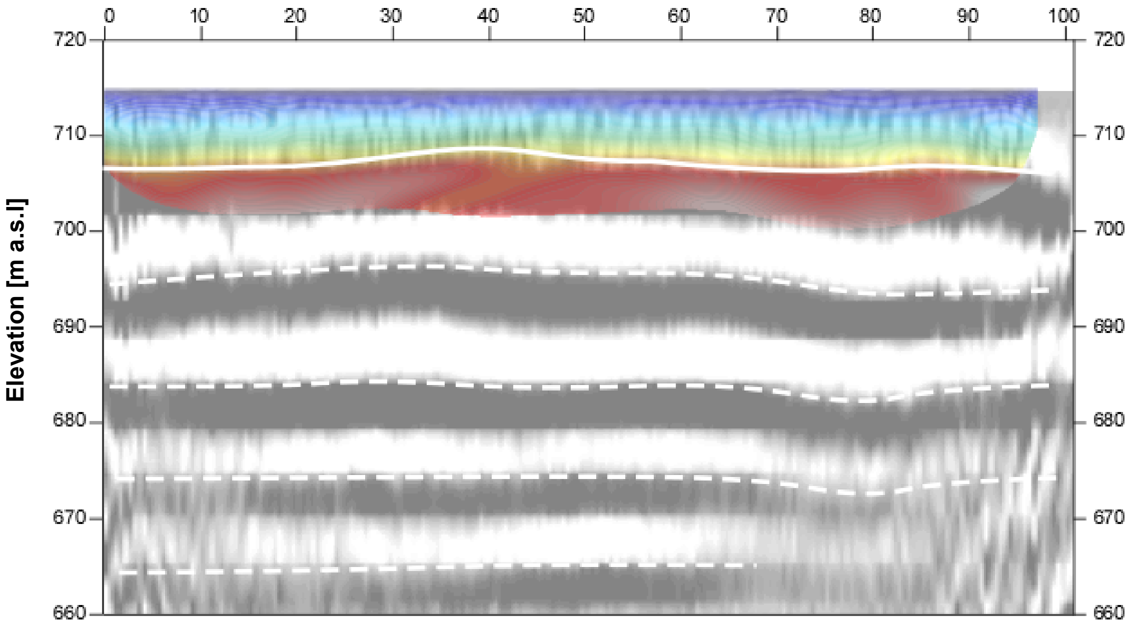

Fig. 3.4d Interpreted hybrid seismic section: The white solid line denotes the bedrock's surface, dashed lines the layering in the bedrock.

3.5 Summary of the results of MASW surveying

In Tab. 3.5a and Fig. 3.5a the mean MASW velocity models from all surveys are given.

Depth	ACB	AIGLE	BALST	BNALP	BOURR	BRANT	FLACH	GIMEL	HASLI	LLS	MUO	PLONS	SKEH	SLE	STEIN	SULZ	TORNY	WEIN	WILA	WIMIS
0.0	496	651	1207	1206	545	773	489	1409	1548	2968	982	1134	178	694	261	1077	456	619	483	993
1.0	496	651	1226	1233	545	797	489	1438	1548	2968	1004	1340	178	694	255	1077	456	619	521	993
2.0	510	707	1236	1132	545	797	499	1432	1548	2989	974	1242	155	699	273	1096	302	635	543	904
3.0	508	722	1254	1128	573	865	488	1416	1585	2978	974	1242	135	699	273	1096	420	634	543	826
4.0	508	655	1246	1135	573	865	472	1381	1585	2928	947	1261	135	697	301	1128	364	636	467	841
5.0	468	671	1276	1291	537	769	443	1331	1529	2928	947	1261	179	697	301	1128	364	619	467	991
6.0	468	614	1243	1291	537	769	416	1274	1529	2849	927	1219	179	678	293	1144	505	603	446	991
7.0	466	614	1244	1344	537	752	411	1274	1442	2849	927	1219	227	678	293	1144	505	569	455	1223
8.0	466	775	1244	1344	497	771	411	1225	1395	2762	908	1219	227	655	330	1121	520	569	466	1223
9.0	500	678	1197	1344	497	771	411	1199	1395	2762	954	1175	227	655	334	1121	595	552	466	1223
10.0	549	678	1141	1470	497	903	472	1199	1325	2762	954	1175	254	655	334	1121	595	552	613	1396
11.0	549	812	1141	1470	497	903	472	1207	1301	2786	954	1175	254	641	413	1041	671	552	659	1396
12.0	638	812	1108	1470	500	1078	472	1283	1301	2786	1064	1389	254	641	472	1041	671	629	659	1396
13.0	638	912	1108	1582	500	1078	472	1283	1301	2786	1064	1389	254	641	472	1041	700	629	659	1485
14.0	708	1025	1079	1755	500	1276	548	1283	1376	3024	1064	1389	300	641	472	1041	700	629	702	1580
15.0	708	1025	1079	1755	500	1276	548	1418	1386	3024	1064	1389	300	642	497	1107	799	629	759	1580
16.0	762	1025	1079	1755	549	1392	663	1579	1386	3024	1260	1534	300	642	533	1107	799	750	759	1580
17.0	841	1264	1191	1846	549	1392	663	1579	1386	3024	1260	1639	300	642	533	1107	865	750	759	1673
18.0	841	1264	1331	2093	549	1537	694	1579	1386	3174	1260	1639	347	642	533	1107	865	750	759	1732
19.0	841	1296	1331	2093	549	1537	694	1579	1603	3174	1260	1639	347	662	533	1107	865	750	831	1732
20.0	743	1296	1331	2093	549	1537	694	1765	1678	3174	1260	1639	347	662	494	1256	950	750	831	1732
21.0	743	1296	1331	2093	709	1537	754	1765	1678	3174	1370	1668	347	662	469	1256	950	741	831	1732
22.0	791	1296	1468	2624	709	1649	754	1857	1678	3174	1370	1743	347	662	469	1256	1123	843	831	1732
23.0	791	1466	1725	2624	709	1649	754	1857	1678	3313	1370	1743	347	662	469	1256	1123	843	831	2132
24.0	791	1552	1725	2737	709	1677	709	1857	1678	3313	1370	1743	383	662	469	1256	1123	843	897	2132
25.0	791	1552	1725	2737	709	1677	709	1857	2018	3313	1370	1743	383	666	586	1256	1123	843	889	2132
26.0	976	1552	1725	2737	709	1677	709	1936	2018	3313	1370	1743	383	666	586	1256	1139	931	889	2132
27.0	976	1552	1725	2737	709	1677	723	1936	2018	3313	1733	2216	383	666	696	1314	1139	931	889	2132
28.0	1072	1552	1985	2737	917	1677	723	1935	2018	3313	1733	2216	383	666	696	1314	1139	1001	889	2132
29.0	1072	1552	1985	2737	917	1744	857	1935	2018	3313	1733	2278	383	666	696	1314	1246	1001	889	2132

Tab. 3.5a Summarized MASW-v_s-models from all surveys.

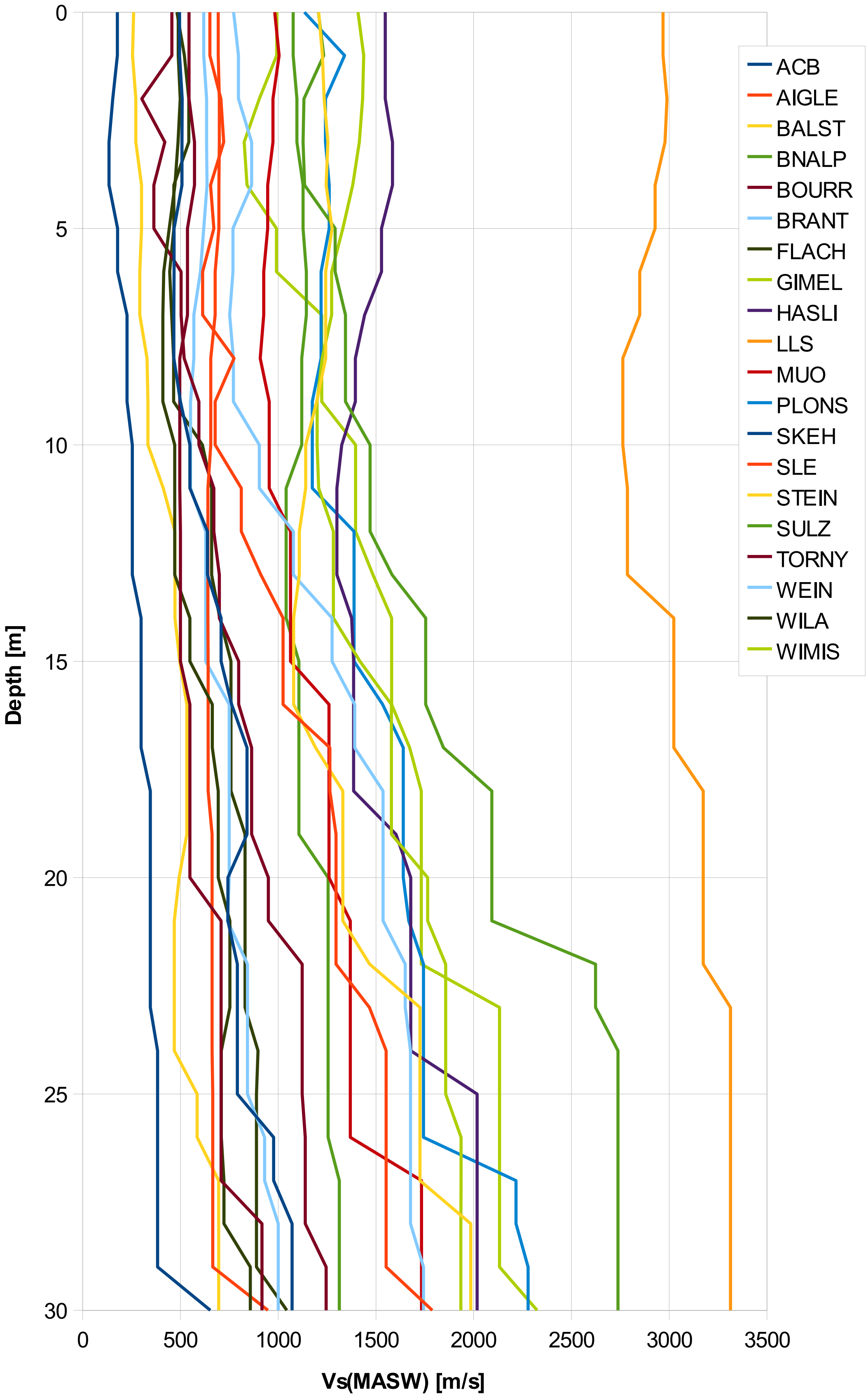

Fig. 3.5a Vs(MASW)-models from all surveys.

In Tab. 3.5b and Fig. 3.5b the MASW velocity scalars $v_{s,5}$, $v_{s,10}$, … from all surveys are given.

Station	Line	Vs,5	Vs,10	Vs,20	Vs,30	Vs,40	Vs,50
ACB	M1	530	516	615	634		
	M2	487	478	556	631		
AIGLE	M1	471	515	738	860		
	M2	825	756	719	839	948	1031
BALST	M1	1364	1362	1321	1411		
	M2	1150	1129	1053	1076		
BNALP	M1	1529	1471	1425	1593		
	M2	732	860	1143	1301		
BOURR		549	513	547	630	694	
BRANT	M1	1733	1597	1591	1781	1864	
	M2	951	856	942	1096	1195	
FLACH	M1	453	423	500	547	549	
	M2	529	497	545	617	644	529
GIMEL	M1	1426	1345	1319	1437	1488	
	M2	1512	1473	1408	1503	1550	
HASLI	M1	1733	1597	1591	1781	1864	
	M2	1395	1337	1292	1375	1493	
LLS		2987	2920	2893	2943	2988	
MUO	M1	862	809	877	970		
	M2	1129	1113	1111	1179		
PLONS	M1	1836	1772	1709	1782	1830	
	M2	641	600	734	888		
SKEH	M1	152	186	236	280		
	M2	155	166	206	239		
SLE		703	695	667	670	683	
STEIN	M1	245	277	333	378		
	M2	283	269	333	373		
SULZ	M1	1194	1185	1123	1201		
	M2	1027	1025	1072	1120		
TORNY	M1	378	417	538	665	722	
	M2	330	426	587	704		
WEIN	M1	500	480	571	633		
	M2	648	586	639	670	702	
WILA	M1	575	575	659	700		
	M2	363	362	487	579		
WIMIS	M1	1137	1112	1308	1433	1384	
	M2	689	774	990	1132		

Tab. 3.5b Summarized MASW-$v_{s,5}$-, $v_{s,10}$, … values from all surveys.

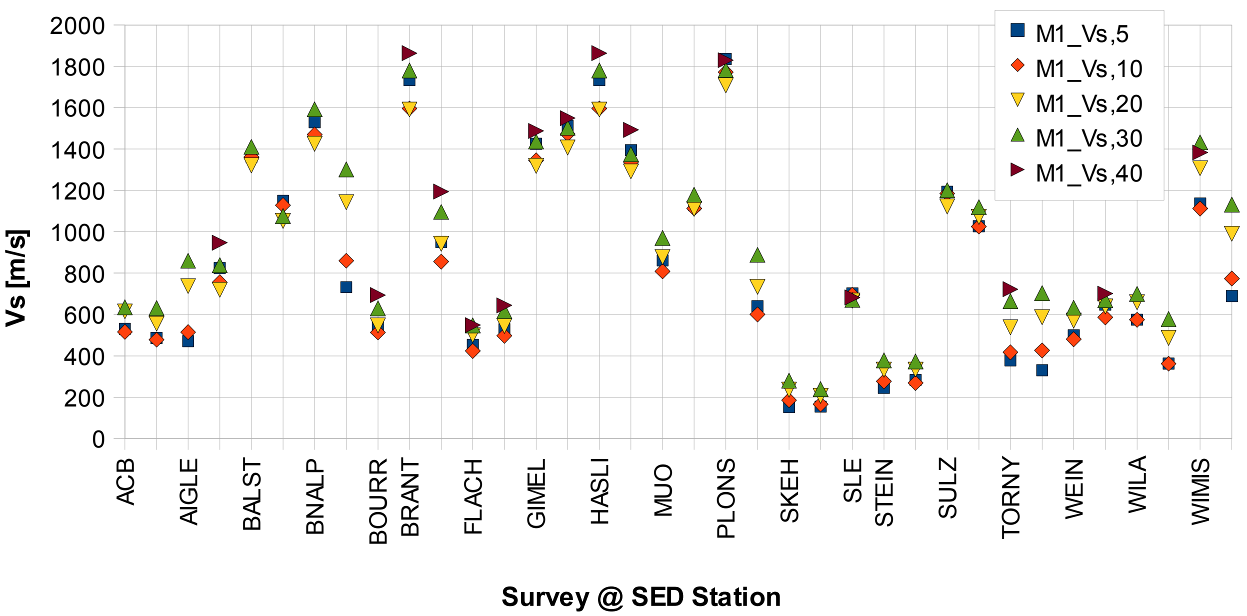

Fig. 3.5b: MASW-derived $v_{s,5}$-, $v_{s,10}$-, … values from all surveys. The values from LLS are skipped in the diagram due to its extraordinary high values.

3.6 Summary of the results of shear wave refraction tomography

In Tab. 3.6 and Fig. 3.6 the mean refraction tomography shear wave velocity models from all surveys are given.

Depth	ACB	AIGLE	BALST	BNALP	BOURR	BRANT	FLACH	GIMEL	HASLI	LLS	MUO	PLONS	SKEH	SLE	STEIN	SULZ	TORNY	WEIN	WILA	WIMIS
0.0	270	479	155	348	342	227	181	315	444	2074	180	459	278	783	200	825	258	128	547	703
1.0	294	501	333	456	342	227	181	534	674	2517	376	459	320	904	201	851	285	136	559	993
2.0	428	695	607	536	380	457	232	796	1138	2954	496	613	479	1173	235	1107	285	238	509	1191
3.0	560	1023	825	618	421	457	232	1056	1570	2987	630	613	851	1191	272	1269	340	332	568	1337
4.0	641	1210	1068	762	421	760	351	1285	1151	2976	743	780	1019	1214	289	1361	397	371	642	1414
5.0	626	1372	1237	907	467	863	351	1485	1228	2984	802	1337	1165	1273	298	1413	475	456	723	1567
6.0	595	1654	1365	1106	467	1109	501	1649	1266	3002	883	1337	1346	1455	306	1429	535	387	817	1632
7.0	688	1838	1423	1239	556	1093	501	1725	1289	2991	883	1295	1372	1631	317	1409	622	391	900	1676
8.0	787	1852	1357	1306	575	1093	650	1648	1302	2931	888	1295	1383	1663	327	1409	719	412	980	1696
9.0	862	1793	1205	1511	575	1280	658	1758	1323	2837	903	1032	1414	1574	351	1394	812	432	1056	1640
10.0	934	1780	1094	1658	593	1327	674	1866	1416	2692	924	1032	1500	1453	381	1431	870	459	1134	1622
11.0	1078	1725	1066	1906	593	1554	674	2004	1422	2623	955	996	1620	1384	404	1446	955	459	1187	1638
12.0		1675	1069	2130	617	1607	737	2192	1414	2558	1012	1040	1667	1383	419	1426	1007	483	1224	1804
13.0		1664	1122	2265	667	1585	776	2220	1438	2633	1011	1040	1702	1466	439	1453	1053	495	1234	1838
14.0		1689	1185	2107	667	1616	776	2315	1467	2735	1082	1081	1743	1595	453	1476	1102	495	1273	1885
15.0		1729	1239	2101	733	1645	807	2398	1502	2845	1129	1081	1782	1746	468	1495	1117	517	1298	1940
16.0		1748	1266	2217	816	1734	807	2489	1547	2982	1216	1132	1861	1925	486		1103	567	1290	2090
17.0		1776	1306	2500	816	1910	844	2577	1585	3192	1250	1132	1893	2117	505		1118	567	1335	2177
18.0		1787	1334	2500	883	2151	884	2679	1637	3355	1304	1277	1826	2342	519		1085	609	1414	2364
19.0		1816	1385		883	2144	884	2636	1719	3495	1323	1787	1841		540		958	609	1494	
20.0		1836	1435		856	2329	925	2738	1759	3553	1353	2077	1943		574		958	649	1552	
21.0		1878	1491		774	1849	958	2858	1802	3606	1372	3479	1871		616		975	689	1556	
22.0		1915	983		774	1849	958	2987	1848	3634	1384	3479	1926		683		992	689	1539	
23.0		1974	1006		728	1993	992	3134	1893	3664	1405	4532	2054		723		1007	762	1474	
24.0		2027	1027		728	1993	992	3217	1916	3701	1394	4532	2142		738		1036	762	1403	
25.0		2080	1049		725	1993	1034	3377	1946	3745	1374	4390	2361		768		1064	837	1376	
26.0		2147	1101		753	2143	1069	3518	2029	3797	1392	4368	2410		679		1097	923	1410	
27.0		2196	1137			2143	1093		2080	3858		3070	2430		705		1137	923	1486	
28.0		2268	1196			2274	1090		2135	3919		3762	2431				1170	1039	1584	
29.0		2315	1276			2274			2193	3985			2430				1191	1039	1671	

Tab. 3.6 Summarized refraction tomographic v_S-models from all surveys.

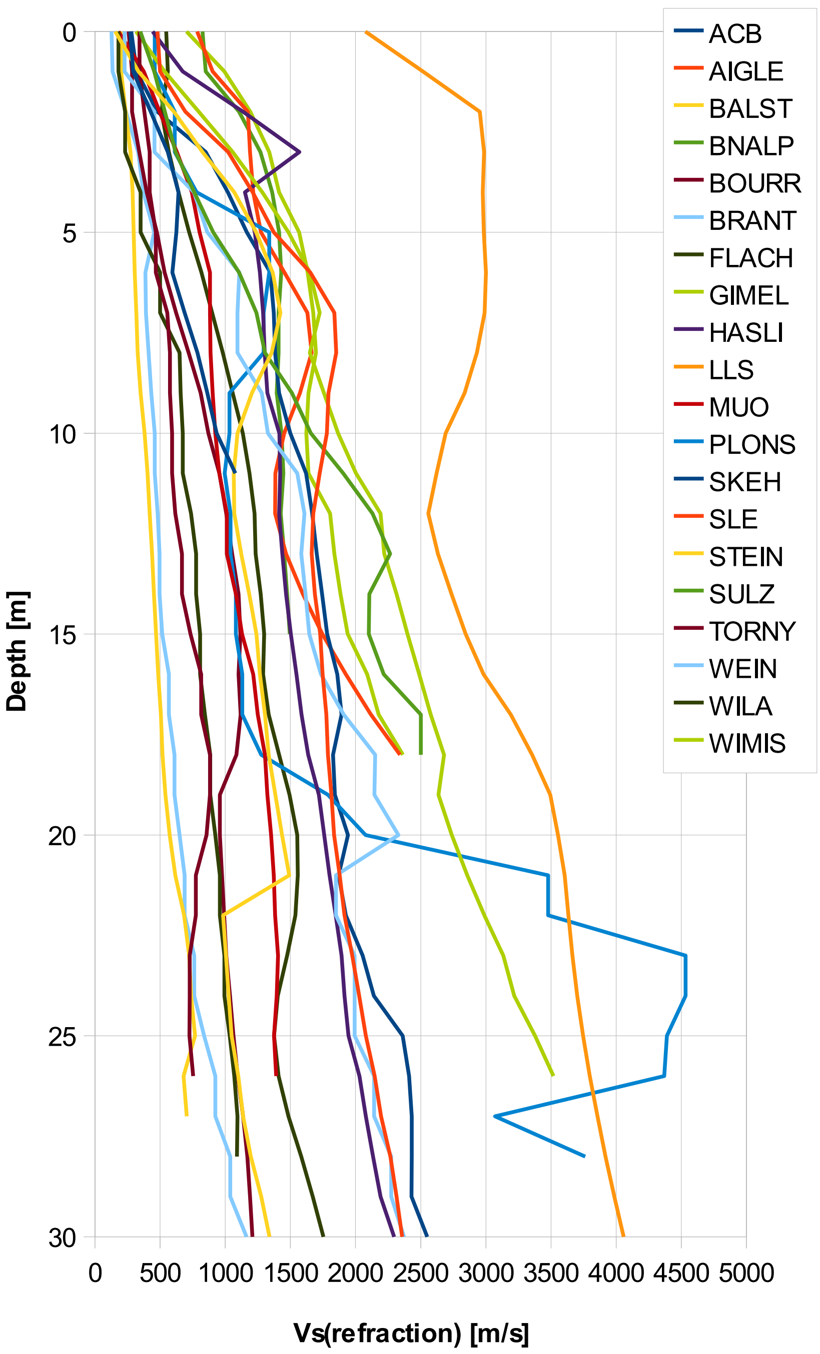

Fig. 3.6 Refraction tomographic shear wave velocity v_S-models from all surveys.

3.7 Summary of the results of compressional wave refraction tomography

In Tab. 3.7 and Fig. 3.7 the mean of refraction tomography compressional velocity models from all surveys are given.

Depth	ACB	AIGLE	BALST	BNALP	BOURR	BRANT	FLACH	GIMEL	HASLI	LLS	MUO	PLONS	SKEH	SLE	STEIN	SULZ	TORNY	WEIN	WILA	WIMIS
0.0	457	248	315	630	382	285	151	707	799	2512	422	378	792	933	401	1388	228	158	432	1222
1.0	543	512	315	630	382	285	271	707	1479	2598	422	524	1049	1234	401	1553	365	306	545	1222
2.0	725	930	477	839	431	425	394	1036	1907	2738	512	1663	1382	1549	494	1943	586	513	683	2125
3.0	912	1583	653	1091	757	832	487	1228	2025	2875	755	2559	1829	1786	614	2176	721	609	927	2701
4.0	1190	1848	1093	1376	757	1278	644	1727	1799	3005	973	3534	2023	1937	730	2261	934	798	1020	3202
5.0	1410	1891	1625	1783	1058	1689	805	1948	1747	3132	1235	4023	2495	2083	899	2039	1250	836	1166	3266
6.0	1674	1980	1781	2099	1234	1917	1008	2401	1566	3271	1396	4830	2749	2260	991	2019	1409	878	1222	3547
7.0	1801	2112	2304	2434	1234	2335	1069	2756	1638	3439	1439	5015	3132	2374	1090	2102	1718	930	1332	4052
8.0	1914	2185	2412	2752	1250	2658	1101	3159	1713	3644	1417	4972	3177	2391	1274	2207	1857	1087	1393	4465
9.0	1901	2286	2791	3142	1294	2793	1114	3472	1711	3857	1424	4997	3196	2352	1391	2252	2074	1209	1504	4528
10.0	1957	2469	3018	3538	1294	2823	1123	3968	1770	4088	1415	5183	3265	2263	1508	2325	2158	1341	1595	4403
11.0	2023	2513	3013	3902	1417	2889	1147	3958	1844	4345	1349	5033	3341	2109	1673	2364	2264	1459	1699	4459
12.0	2103	2424	3170	4445	1417	2964	1199	4331	1918	4622	1375	5228	3365	2012	1735	2383	2297	1627	1774	4682
13.0	1968	2352	3169	4549	1577	2954	1285	4564	1980	4910	1485	5493	3380	2110	1758	2420	2334	1710	1869	5026
14.0	1968	2432	3276	4620	1749	2982	1389	4984	1992	5179	1583	5546	3546	2255	1866	2455	2412	1789	1950	5598
15.0	2020	2577	3393	4693	1749	3055	1469		2154	5408	1693	5534	3689	2315	1959	2508	2486	1812	2055	5886
16.0	2061	2951	3460	4801	1919	3159	1533		2576	5585	1733	5526	3850		2219	2555	2241	1852	2147	
17.0	2086	3093	3578	3915	2082	3200	1597			5728	1772	5621	3977		2364	2693	2289	1872	2305	
18.0	2093	3119	3557	4167	2082	3297	1635			5862	1780		4017			2714	2284	1922	2388	
19.0	2083	3060	3551	4543	2247	3236	1656			5995	1816		4032			2773	2240	1955	2548	
20.0		2998	3551	4865	2414	3461	1670			6104	1842		3882			2824	2220	2245	2633	
21.0		2942	3520	5028	2414	3377	1691			6181	1914		4035			2835	2106	1555	2773	
22.0		3080	3636	5139	2560	3501	1719			6217	1958		4215			2862		1594	2889	
23.0		3275	3634	5329	2560	3608	1766			6231	2149		4232			2878		1659	3022	
24.0		3565	3771		2692	3714	1914				2190		4088			2575		1726	3126	
25.0			3847		2817	3714	1955				2233		3951			2841		1782	2705	
26.0			3884		2817	3808	1965				2277		3832			2841		1842	2821	
27.0			3941		2923	3857	1975				2323					2857		1896	2878	
28.0			3984		2923	3869	1977				2363					2857		1954	2993	
29.0			4136		2933	3869	1971				2411					2922		2010	3050	

Tab. 3.7 Summarized refraction tomographic v_P-models from all surveys.

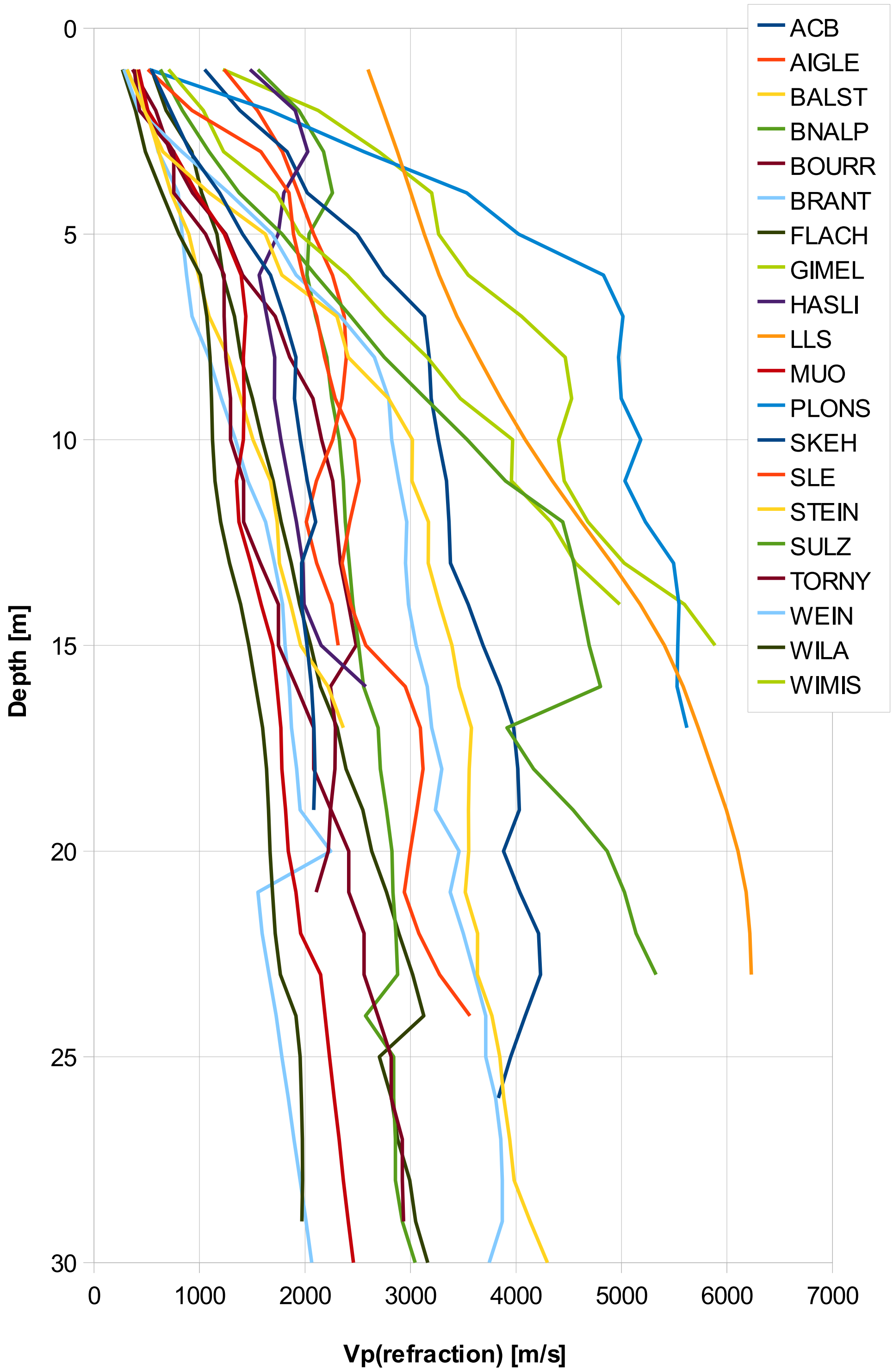

Fig. 3.7 Refraction tomographic compressional wave velocity v_p-models from all surveys. Steps in the velocities are caused by different obtained depths of results and highly different velocities between line 1 and line 2.

4 ERROR ESTIMATES

Due to methodological differences, v_s velocities derived by MASW analysis and by the refraction tomography technique may differ considerably. This is because MASW analysis cannot image small rock/soil inhomogeneities as a dispersion image with an array length of i.e. 40-m only yields one single v_s-value at each depth. On the other hand, refraction diving wave tomography results produce v_s-sections with a high lateral resolution, but fail to provide information at greater depths.

The error values given in Tab. 4.1 below are a rough overview over the estimated errors for all surveys. More detailed information about errors in specific survey refer to the respective report in appendices.

Surveying method	Type of result	Error estimate
v_s – refraction tomography	v_s – velocity field image	10 – 20 %
MASW only "+" or only "-" values*	v_s – velocity field image	10 – 25 %
MASW (mean of "+" & "-" values)*	v_s – velocity field image	8 – 15 %
v_p – refraction tomography	v_p – velocity field image	5 – 12 %
Reflection seismic surveying	Image of subsurface structures	n.a.

** MASW values in the uppermost 6 m are usually prone to an error of about 20 to 40 % (only one direction) resp. 10 – 20 % (mean of both directions).*

Tab. 4.1 Error estimates for the methods applied. Note that higher error estimates are to be taken into account with increasing depths.

The above error estimates are of a qualitative character only. In view of the intense fluctuations to be expected in both the lateral and vertical directions, any attempt to derive a quantitative general error estimate to be valid for the entire survey is to be considered as futile. In particular possibly existing military bunkers and galleries below the survey site (in which the earthquake monitoring station is positioned) on both seismic lines have a certain impact on the quality of dispersion images. Nevertheless, all velocity data coincide well, independently of the methodological differences.

In most surveys, the uppermost ~4-6 m, the MASW derived shear wave velocities are considerably higher than the refraction tomography values. In greater depths, they correspond well.

To compare the quality of vs-models derived in this project, the Tab. 4.2 gives an overview of mean values of all vs(refraction)- and vs(MASW)-models and the respective deviation of percentage.

Depth [m]	ACB		AIGLE		BALST		BNALP		BOURR		BRANT		FLACH		GIMEL		HASLI		LLS		MUO		PLONS		SKEH		SLE		STEIN		SULZ		TORNY		WEIN		WILA		WIMIS	
	Vs	MD	Vs	MD	Vs	MD	Vs	MD	Vs	MD	Vs	MD	Vs	MD	Vs	MD	Vs	MD	Vs	MD	Vs	MD	Vs	MD	Vs	MD	Vs	MD	Vs	MD	Vs	MD	Vs	MD	Vs	MD	Vs	MD	Vs	MD
	[m/S]	[%]	[m/S]	[%]	[m/S]	[%]	[m/S]	[%]	[m/S]	[%]	[m/S]	[%]	[m/S]	[%]	[m/S]	[%]	[m/S]	[%]	[m/S]	[%]	[m/S]	[%]	[m/S]	[%]	[m/S]	[%]	[m/S]	[%]	[m/S]	[%]	[m/S]	[%]	[m/S]	[%]	[m/S]	[%]	[m/S]	[%]	[m/S]	[%]
0.0	383	29	565	24	681	77	777	55	443	23	500	55	387	35	862	63	996	55	2521	18	581	69	797	65	228	32	738	6	230	13	993	11	357	33	374	66	515	52	848	20
1.0	395	26	576	23	780	57	844	46	444	23	512	56	387	35	986	46	1111	39	2742	8	690	46	899	53	249	29	799	13	228	12	1002	10	371	26	378	64	540	45	993	17
2.0	469	9	701	16	922	34	834	45	463	18	627	29	410	29	1114	29	1343	23	2971	1	735	33	928	50	317	51	936	25	254	10	1100	4	293	21	436	45	526	35	1048	20
3.0	534	16	872	25	1040	21	873	40	497	15	661	31	403	28	1236	15	1578	24	2983	0	802	21	928	50	493	73	945	26	273	6	1154	7	380	18	483	31	555	32	1081	24
4.0	575	19	933	37	1157	12	949	33	497	15	812	8	432	12	1333	4	1441	15	2952	1	845	16	1021	38	577	77	955	27	295	3	1205	9	381	23	504	26	554	38	1128	25
5.0	547	14	1022	36	1256	11	1099	19	502	7	816	6	413	14	1408	8	1428	12	2956	1	874	14	1299	31	672	73	985	29	299	3	1223	10	420	22	537	17	595	40	1279	23
6.0	531	12	1134	47	1304	10	1199	15	502	7	939	18	444	9	1461	13	1441	11	2925	3	905	15	1278	29	763	77	1066	36	299	9	1239	11	520	13	495	22	631	46	1312	24
7.0	577	19	1226	50	1334	14	1292	7	547	2	923	19	441	9	1499	15	1391	6	2920	2	905	17	1257	28	799	72	1154	41	305	10	1232	11	563	10	480	21	678	50	1449	16
8.0	627	26	1314	41	1300	12	1325	4	536	7	932	17	491	22	1437	15	1364	7	2846	3	898	17	1257	28	805	72	1159	43	328	3	1217	11	619	16	490	20	723	52	1460	16
9.0	621	26	1235	45	1201	13	1428	6	536	7	1026	27	493	22	1479	19	1371	7	2800	1	928	14	1103	25	821	72	1115	41	343	3	1212	10	704	15	492	16	761	57	1431	15
10.0	678	25	1229	45	1118	19	1564	7	545	9	1115	21	539	17	1533	22	1355	4	2727	1	939	12	1103	25	877	71	1054	38	357	7	1224	11	733	19	521	16	873	53	1509	10
11.0	726	32	1269	36	1103	23	1688	13	545	9	1229	27	539	17	1605	25	1341	6	2704	3	954	10	1085	25	937	73	1013	37	408	10	1176	15	813	17	521	16	923	54	1517	8
12.0	638	14	1244	35	1089	28	1800	18	559	10	1343	20	560	21	1737	26	1339	6	2672	4	1038	5	1214	20	961	74	1012	37	446	6	1169	15	839	20	581	11	942	57	1600	13
13.0	638	14	1288	29	1115	30	1923	18	584	14	1331	19	573	24	1751	27	1346	6	2709	3	1037	6	1214	20	978	74	1054	39	455	4	1178	16	876	20	585	10	947	56	1661	11
14.0	708	3	1357	24	1132	30	1931	9	584	14	1446	14	624	20	1799	29	1406	8	2880	5	1073	3	1235	19	1021	71	1118	43	463	2	1186	16	901	22	585	10	987	54	1682	8
15.0	708	3	1377	26	1159	31	1928	9	617	19	1460	13	635	20	1908	26	1425	8	2934	3	1096	4	1235	19	1041	71	1194	46	483	5	1236	14	958	17	592	8	1029	50	1700	9
16.0	762	10	1387	26	1173	31	1909	11	683	20	1563	11	711	9	2034	22	1440	9	3003	1	1245	4	1333	15	1080	72	1284	50	509	5	1107	3	951	16	689	12	1025	48	1750	13
17.0	841	0	1520	17	1249	24	2064	14	683	20	1651	16	723	11	2078	24	1452	9	3108	3	1256	3	1386	19	1096	73	1380	53	519	3	1107	3	992	15	689	12	1047	47	1841	12
18.0	841	0	1526	17	1332	27	2228	8	716	23	1844	18	757	11	2129	26	1470	10	3265	3	1274	4	1458	16	1086	68	1492	57	526	3	1107	3	975	12	703	9	1087	49	1943	14
19.0	841	0	1556	17	1358	26	2093	5	716	23	1841	18	757	11	2107	25	1642	16	3335	5	1281	4	1713	27	1094	68	662		537	4	1107	3	896	8	703	9	1163	48	1155	67
20.0	743	13	1566	17	1383	26	2093	5	703	22	1933	24	771	13	2252	22	1705	12	3364	6	1291	5	1858	17	1145	70	662		534	9	1256	3	953	11	716	8	1192	48	1732	5
21.0	743	13	1587	18	1411	26	2093	5	742	4	1641	11	822	11	2311	24	1719	12	3390	6	1370	4	2573	35	855	79	662		542	14	1256	3	958	12	724	5	1194	46	1732	5
22.0	791	19	1605	19	1306	17	2624	17	742	4	1716	5	822	11	2422	23	1735	13	3404	7	1374	4	2611	33	873	80	662		576	19	1256	3	1079	5	792	10	1185	43	1732	5
23.0	791	19	1720	15	1485	26	2624	17	719	1	1764	9	833	13	2495	26	1750	13	3488	5	1381	5	3137	44	916	83	662		596	21	1256	3	1084	5	816	7	1153	40	2132	13
24.0	791	19	1790	13	1492	25	2737	12	719	1	1782	8	803	16	2537	27	1758	14	3507	6	1378	4	3137	44	969	81	662		603	22	1256	3	1094	4	816	7	1150	34	2132	13
25.0	791	19	1816	15	1499	25	2737	12	717	1	1782	8	817	18	2617	29	1994	11	3529	6	1371	4	3066	43	1043	84	666		677	16	1256	3	1103	2	841	5	1132	33	2132	13
26.0	976	4	1850	16	1517	24	2737	12	731	3	1832	11	829	19	2727	29	2022	10	3555	7	1377	4	3056	43	1059	85	666		617	14	1256	3	1125	2	929	2	1149	34	2132	13
27.0	976	4	1874	17	1529	23	2737	12	709		1832	11	846	19	1936	4	2038	11	3585	8	1733	10	2501	15	1066	85	666		699	1	1314	7	1138	0	929	2	1187	37	2132	13
28.0	1072	6	1910	19	1722	20	2737	12	917		1876	14	845	19	1935	4	2057	11	3616	8	1733	10	2732	25	1066	85	666		696	2	1314	7	1149	1	1013	4	1237	40	2132	13
29.0	1072	6	1934	20	1749	18	2737	12	917		1920	12	857	5	1935	4	2076	12	3649	9	1733	10	2278	4	1066	85	666		696	2	1314	7	1228	7	1013	4	1280	43	2132	13
30.0	1072	6	2072	14	1770	16	2737	12	917		1953	14	857	5	1935	4	2110	13	3686	10	1733	10	2278	4	1285	66	947		696	2	1314	7	1233	6	1055	7	1399	39	2325	4
Mean		14		26		25		16		10		18		17		22		13		5		12		29		72		22		8		8		14		16		45		15

Tab. 4.3: Mean shear wave velocity values (v_S) from MASW and refraction velocity derivation at each station and the corresponding mean deviation percentage (MD).

5 SUMMARY AND CONCLUSIONS

- From December 2008 until June 2009, combined seismic s- and p-wave surveys have been carried out at 20 SED earthquake monitoring stations in various parts of Switzerland, in the Jura range, the foreland basin, the Prealps and in the Alps.
- In the close vicinity of the 20 earthquake monitoring stations, 2 – ideally – perpendicular seismic profiles have been surveyed with both horizontal and vertical sensors.
- The shear wave data sets have been evaluated by conventional diving wave refraction tomography techniques in order to derive the s-wave velocity field along the seismic line.
- The p-wave data sets have been processed
  - firstly, to derive a 2D s-wave velocity field by using the MASW (Multichannel Analysis of Surface Waves) technique;
  - and secondly, according to the hybrid seismic data processing scheme for representing the subsurface structures in a combined reflection seismic section with the superimposed p-wave velocity field.
- Based on the MASW results, the scalars $v_{s,5}$, $v_{s,10}$, $v_{s,20}$ ... have been calculated as functions of profile meter and as 1D shear wave velocity models effective for the SED earthquake monitoring stations.
- The shear wave refraction velocities, the compressional wave refraction velocities, the MASW inversion velocities and the maximum shear wave velocities calculated from the compressional wave refraction velocities have been correlated for assessing the accuracy of the obtained values.

Schwerzenbach, 24th July 2009

Walter Frei	Lorenz Keller
dipl. Natw. ETH	dipl. Natw. ETH
managing director	project manager

BIBLIOGRAPHY

Gebrande H and Miller H., 1985. **Refraktionsseismik** (in German). In: F. Bender (Editor), *Angewandte Geowissenschaften II*. Ferdinand Enke, Stuttgart; pp. 226-260.

Gebrande, H., 1986. **CMP-Refraktionsseismik.** In: L. Dreses et al.; *Symposium: Seismik auf neuen Wegen* sponsored by Dt. Vereinigung d. Erdölgeol. u. Erdöling., Celle, 191-205

Park, C.B., Miller R.D., and Xia, J., 1996: **Multi-channel analysis of surface waves using Vibroseis.** Exp. Abs., Soc. Expl. Geophys., p. 68—71.

Park, C.B., Miller, R.D., and Xia, J., 1998, **Multichannel analysis of surface waves.** *Geophysics*, vol. 64, n. 3, p. 800-808.

Park, C.B., Miller, R.D., and Xia, J., 1999, **Imaging dispersion curves of surface waves on mulit-channel record.** In: *68th Ann. Internat. Mtg. Soc. Expl. Geophys.*, Expanded Abstracts, p. 1377-1380..

Schuster, G. T. and Quintus-Bosz, A., 1993: **Wavepath eikonal traveltime inversion: Theory.** *Geophysics*, vol. 58, p.1314-1323, DOI:10.1190/1.1443514.

Watanabe, T.; Matsuoka, T. and Ashida, Y., 1999: **Seismic traveltime tomography using Fresnel volume approach.** *SEG Expanded Abstracts* 18, pp. 1402, DOI:10.1190/1.1820777.

Xia, J., R.D. Miller, and C.B. Park, 1999: Estimation of near-surface shear-wave velocity by inversion of Rayleigh wave. Geophysics, vol. 94, p. 691-700.